EVALUATION OF STRUCTURAL CAPACITY OF EPOXY-COATED CONCRETE PIPES AND ITS INTERACTION WITH SOIL

by

ELMIRA RIAHI

Presented to the Faculty of the Graduate School of
The University of Texas at Arlington in Partial Fulfillment
of the Requirements
for the Degree of

DOCTOR OF PHILOSOPHY

THE UNIVERSITY OF TEXAS AT ARLINGTON
August 2016

Dedication

I dedicate this dissertation to my beloved parents for their endless love, encouragement and support throughout my life that kept me motivated to experience new things and expand my world through knowledge.

Acknowledgements

First, I want to express my deepest gratitude and acknowledgement to my advisor, Dr. Xinbao Yu, for his endless support and encouragement in the past four years. I learned a lot from him, and this research could not be done without his guidance.

I also would like to thank my committee members Dr. Anand Puppala, Dr. Simon Chao and Dr. Mohammad Najafi for their valuable comments, help and time. I am thankful to Dr. Xinbao Yu, Dr. Ali Abolmaali, Dr. Laureano Hoyos, Dr. Sahadat Hossain and Dr. Chein-Pai Han for fulfilling my experience at University of Texas at Arlington by sharing their knowledge during my course work in the geotechnical engineering program.

I would also like to thank my brother and friends for their love and encouragement. Without my family and friends, none of the achievements that have come with this amazing journey could have happened.

July 21, 2016

Abstract

EVALUATION OF STRUCTURAL CAPACITY OF

EPOXY-COATED CONCRETE PIPES

AND ITS INTERACTION WITH SOIL

by

Elmira Riahi, PhD

The University of Texas at Arlington, 2016

Supervising Professor: Xinbao Yu

Rehabilitation of concrete structures by using synthetic resins such as epoxy is increasing worldwide. Understanding the structural behavior of the resultant composite structure and the interaction between the coating and concrete can be beneficial in predicting performance of the rehabilitated structure. However, very little is known about the strength of the epoxy-coated concrete. This researcher conducted laboratory experiments designed to evaluate epoxy coated concrete specimens under different load configurations with an emphasis on its stress-strain characteristics. The tests include uniaxial compression cylindrical specimens, three-point and four-point bending and tests on beam specimens and three-edge bearing tests on concrete pipe specimens. The concrete specimens used in the tests consisted of concrete specimens with and without epoxy coating. Finite element modeling (FEM) was adopted to simulate the epoxy-coated concrete beams and pipes under three-point and four-point bending and three-edge bearing tests. The FEM models were verified by test results and simulated the behavior of epoxy-coated concrete under different load configurations. Parametric study on a

concrete calibrated model showed that increasing the thickness of the lining for higher degrees of deterioration of concrete has more effect on increasing the peak load carried by the pipe. Deteriorated manholes repaired with epoxy liner were selected as another application example and simulated by ABAQUS using the calibrated material models to evaluate its structural performance under soil, water, and traffic loads. Parametric study results for rehabilitated manhole structures indicates that for partially deteriorated manholes the epoxy linings do not have a significant effect on the radial deformation of the manhole structure and in the case of fully deteriorated manholes increasing the thickness of the lining can result in smaller radial deformations.

Table of Contents

List of Illustrations

List of Tables

Chapter 1

1.1 Introduction

By definition infrastructures are “the basic physical and organizational structures and facilities (e.g., buildings, roads, and power supplies) needed for the operation of a society or enterprise” (1). These “basic structures” are aging throughout the world and they need immediate attention to minimize their repair or replacement cost. Grade D+ was reported by ASCE in their latest 2013 report card on infrastructure in the United States. Wastewater and drinking water systems received a D with an estimated $298 billion projected as the cost for wastewater improvement over the next 20 years and over $1 trillion for drinking water pipes replacement (2) makes it clear enough why more research and effort must be made in this area.

This dissertation focuses on concrete pipes and manholes used in sewer systems as part of a water system rehabilitation study. Gravity flow wastewater and storm water collection systems consist of sewer pipes, manholes and transmission components (3). Commonly used materials in the sewer system include polyvinyl chloride (PVC) pipe, concrete cylinder pipes, and ductile or cast iron pipes. There are about 740,000 miles of sewer network in the United States, and most of that network was installed after World War II, which means the post-war pipes are close to the end of their service life. 44% of the sewer network is made of clay or concrete pipes (4). The other component of the sewer system, manholes, number 20 million in the United States and 4 million (20%) of them are at least 50 years old (3).

Various methods are available to address concrete pipe deterioration. For instance replacement of the deteriorated pipe or manhole structure which can be difficult and expensive in many cases, chemical grouting in which chemical materials such as acrylamide or urethane grout are applied under pressure into joints and/or surrounding

soil, pipe linings which are inserted inside the existing pipe to restore it structurally and finally coatings that are applied inside of the pipe to protect it from corrosion and abrasion (5).

The spray-on lining method is a trenchless rehabilitation method for pipes and manholes. In this method a layer of lining is sprayed inside of the deteriorated pipe. In general, the linings used in this method are divided into two main categories: cementitious materials and polymers. According to the United States Environmental Protection Agency (EPA) (6) , the main advantage of using cementitious lining is its cost effectiveness and the fact that reinforcement can be used with this type of lining. But this material is not as corrosion-resistant as polymer linings. For polymer linings, high-build polymer is available for sewer rehabilitation and bonding is not an issue when using this type of lining. The main disadvantage of polymer linings is the importance of surface preparation before applying the lining which can be difficult in the case of pipes with small diameters (7). Different polymers used in this method are epoxies, polyurethanes and polyureas. The focus of current research is mainly on epoxy linings.

Epoxy resins were first commercialized in Europe and the United States in the late 1930's. Epoxy resins are a class of thermoset materials which are routinely used as adhesive coatings, encapsulates, casting material, potting compounds, and binders. The simplest formulation of epoxy consists of a single epoxy resin, which is formed by the reaction of bisphenol and epichlorohydrin, and a curative. More complex formulations that can improve the properties of the material according to the requirements may include multiple resins, modifiers and a curative package that drives specific reactions at specific times (8).

The cost of applying epoxy lining is between $5 to $10/ft, which is based on diameter. The experience required for applying the lining is categorized as medium

experience, which means 10 to 20 years. When comparing the cost and experience requirements for epoxy lining with the cost and experience requirements for cementitious lining, both are categorized in the same group (9).

Epoxy lining started being used instead of cement mortar lining in pipes in the late 1970s and early 1980s. Epoxy lining was officially approved in 1985 in the United Kingdom. By 1995, it was well established in the U.K., Japan, Sweden and Germany, while still new and innovative in the United States. By 2010, 10% of pipe coatings were performed using epoxy in the United States (10). In this rehabilitation method with polymeric linings, a layer of material is sprayed inside of the deteriorated concrete pipe or manhole structure.

1.2 Problem Statement and Research Objectives

Existing literature on epoxy-coated concrete mainly focuses on bonding and durability performance. In 2005, Liu and Vipulanandan performed 79 laboratory and 16 in-situ tests on four different commercially available epoxy-based coatings to study tensile bonding strength of epoxy to dry and wet concrete substrate (11). In 2003, A.A. Almusallam et al. studied the effect of five generic types of concrete surface coatings, including epoxy, on durability of concrete (12). Compression, tension, flexure, and shear bond tests on concrete specimens repaired by epoxies were conducted by El-Hawary et al. in 1998 to study the effect of variables such as types of cement, types of epoxy, duration of exposure to seawater, and the effect of temperature on the strength of epoxy-repaired concrete (13). However, numerical analyses on epoxy coated concrete is limited, even though generating finite element models of epoxy rehabilitated concrete can help further the effective use of this method for improving strength and durability of deteriorated concrete structures.

Ever since this method was first used for concrete structure rehabilitation, its structural capacity has been ignored. The structural capacity is referred to as the contribution of the epoxy coating to resist structure's design loads. To explain structural behavior of epoxy coated concrete members, stress-strain relations of the composite members under different loading configurations must be understood. Furthermore, the effect of type and thickness of the coating on load bearing capacity of deteriorated concrete pipes or manholes must be clarified. As mentioned before, lack of a numerical model of an epoxy coated member with an appropriate interaction definition between the coating and concrete and material properties in available literature limits the potential of performing a detailed study on various parameters that can ameliorate the knowledge of structural capacity of epoxy coated concrete members.

According to the problem statement, the primary objective of this research was to generate a finite element model to predict the behavior of rehabilitated composite structures. To accomplish this, a thorough study of the structural capacity of rehabilitated concrete members such as pipes and manholes was achieved by means of existing experimental programs and a number of supporting objectives were established and accompanied by research as listed below:

Supporting Objective 1: Testing stress-strain behavior of epoxy-coated members—Experiments were performed to determine the stress-strain behavior of epoxy-coated concrete members under flexural, D-load and circumferential loading configurations.

Supporting Objective 2: Calibration of finite element model—Test results were used to calibrate the finite element model and thereby predict the behavior of epoxy-coated concrete members.

Supporting Objective 3: Defining parameter-behavior relationships—A parametric study was conducted on the various parameters that may affect behavior of the epoxy-coated concrete members.

Supporting Objective 4: Load-bearing study of epoxy-coated concrete manholes—Study behavior of epoxy-coated concrete manhole under different load combinations existing in the field

1.3 Dissertation Organization

This dissertation consists of three manuscripts one of which is a modified version of a published in the ASCE Journal of pipeline systems engineering and practice on December 16, 2015 (14). The other two manuscripts are ready for submission. The dissertation is divided into five chapters: Ch. 1) Introduction, Ch. 2) Experimental and Numerical Analyses of Strength of Epoxy Coated Concrete under Different Load Configurations, Ch. 3) Structural Behavior of Concrete Pipe with Spray-on Cured-in-Place Lining, Ch. 4) Structural Behavior of Epoxy Coated Rehabilitated Concrete Manhole Structure, and Ch. 5) Conclusion.

Chapter 1: This chapter presents an introduction to the present situation of underground infrastructure in the United States and magnifies existing problems that are being addressed in this research. Objectives of the research are also clarified in this chapter.

Chapter 2: A set of laboratory tests are performed on concrete beams and pipes at the laboratory of the University of Texas at Arlington's Center for Underground Infrastructure Research and Education (CUIRE). The results of these tests which were conducted on concrete members with and without linings are used to study the effect of different lining materials on flexural strength of concrete beams and D-load strength of concrete pipes. Multipurpose commercial software, ABAQUS is used to generate a

calibrated finite element model of concrete pipe under D-load test configuration. The model is verified by using the test results and parametric study is performed on interaction behavior between concrete and epoxy lining.

Chapter 3: An additional set of experiments are performed on larger concrete beam specimens to improve the experimental database and previously developed finite element model. This model is used to perform parametric studies on thickness of the lining, percentage of concrete deterioration and material properties of the lining.

Chapter 4: This chapter focuses on rehabilitation of deteriorated concrete manhole structures. The behavior of resultant composite structure after rehabilitation is usually overlooked. In the current research structural capacity of the rehabilitated concrete manhole is studied by generating a finite element model in ABAQUS. The model is calibrated by using the results from an existing full-scale manhole experiment performed by Sabouni in 2008 at the University of Western Ontario, Canada (15). After model validation, a layer of epoxy lining is added to the model and behavior of the composite structure is studied under different loading conditions and different degrees of concrete deterioration with different thicknesses of lining material and property. For this simulation two constitutive models are considered for simulation of the surrounding soil: Mohr-Coulomb which is an existing material model in ABAQUS and Duncan-Chang material behavior, which is implemented in the model as a subroutine.

Chapter 5: Conclusions based on the research are presented and recommendations for future study are offered in this chapter.

References

1. Infrastructure, Google.Inc: www.Google.com.
2. ASCE, Report card for America's infrastructure, 2013: http://www.infrastructurereportcard.org/.
3. Mohammad Najafi, V.F.S., STRUCTURAL CAPABILITIES OF NO-DIG MANHOLE REHABILITATION, 2015.
4. Sterling, Ray,Wang, L., Morrison, R. "White Paper on Rehabilitation of Wastewater Collection and Water Distribution Systems." 2009. Final Report, EPA/600/R-09\046, Office of Research and Development, Washington, DC. nepis.epa.gov/Exe/ZyPURL.cgi?Dockey=P10044GX.TXT
5. Abraham, D.M. and S. Ali Gillani, Innovations in materials for sewer system rehabilitation. Tunnelling and Underground Space Technology, 1999. 14, Supplement 1: p. 43-56.
6. Ray Sterling, J.S., Erez Allouche, Wendy Condit, Lili Wang, State of Technology for Rehabilitation of Wastewater Collection Systems, 2010, United States Environmental Protection Agency.
7. Najafi, M., Trenchless Technology: Planning, Equipment, and Methods. 2012: McGraw-Hill Education.
8. Maureen A. Boyle, C.J.M., and John D. Neuner, Epoxy Resins. 2001.
9. Najafi, M. and S. Gokhale, Trenchless technology : pipeline and utility design, construction and renewal. 2005, New York: McGraw-Hill.
10. Dan Ellison, F.S., Peter Oram, Will Lovins, and Andrew Romer,Steven J. Duranceau,Graham Bell, Global Review of Spray-On Structural Lining Technologies, 2010.

11. Liu, J. and C. Vipulanandan, Tensile bonding strength of epoxy coatings to concrete substrate. Cement and concrete research, 2005. 35(7): p. 1412-1419.
12. Almusallam, A., et al., Effectiveness of surface coatings in improving concrete durability. Cement and Concrete Composites, 2003. 25(4): p. 473-481.
13. El-Hawary, M.M., Evaluation of bond strength of epoxy-coated bars in concrete exposed to marine environment. Construction and Building Materials, 1999. 13(7): p. 357-362.
14. Yu, X., et al., Experimental and Numerical Analysof Strength of Epoxy-Coated Concrete under Different Load Configurations. Journal of Pipeline Systems Engineering and Practice, 2016. 7(2): p. 04015024.
15. Sabouni, R., Experimental Investigation & Numerical Modeling of Concrete Manholes, in Civil and Environmental Engineering2008, The University of Western Ontario: School of Graduate and Postdoctoral Studies.

Chapter 2

Experimental And Numerical Analyses Of Strength Of Epoxy Coated Concrete Beam And Pipe

Abstract

Rehabilitation of concrete structures by using synthetic resins such as epoxy is increasing worldwide. Understanding the structural behavior of the resultant composite structure and the interaction between the coating and concrete can be beneficial in predicting performance of the rehabilitated structure. However, the knowledge of strength of the epoxy-coated concrete is very limited. This paper presents laboratory experiments designed to evaluate epoxy coated concrete specimens under different load configurations with an emphasis on its strength characteristics. The studied load configurations included uniaxial compression for cylindrical specimens, three-point bending for beam specimens, and three-edge bearing for concrete pipe specimens. The concrete specimens used in the tests consisted of concrete specimens with and without epoxy coating. Finite element modeling (FEM) was adopted to simulate the epoxy-coated concrete beams and pipes under three-point bending and three-edge bearing loads. The FEM models were verified by test results and simulated the behavior of epoxy-coated concrete under different load configurations.

2.1 Introduction

Concrete structures experience deterioration when they are exposed to severe environmental and mechanical loading. The number of structures that have deteriorated in service and stand in need of repair and maintenance is vast and ever increasing with one in nine US bridges rated as structurally deficient. The overall number of high-hazard dams was estimated at approximately 14,000 in 2012. Roads received a grade of D in 2013 with a Federal Highway Administration estimate of an unreachable $170 billion said

to be needed annually to fix the problems. The common denominator of all these failing structures is concrete. Different repair methods are suggested for concrete structures according to the degree of deterioration. One of the most recent and developing methods is using synthetic resins. Synthetic resins such as epoxy, polyester, acrylic, and polyurethane have found various applications in civil engineering. Epoxy resins, first commercialized in 1946, are one of the most important and widely used types of polymeric systems. These epoxy resin system are used in civil engineering works such as grouting of cracks, repairs of eroded concrete structures, emergency repairs of bridges, aqueducts, chemically corroded columns and beams (Saxena 2014).

Existing literature on epoxy-coated concrete mainly focuses on bonding (Liu and Vipulanandan 2005) and durability performance (El-Hawary et al. 1998). Liu and Vipulanandan (2005) studied tensile bonding strength of epoxy to dry and wet concrete substrate by performing 79 laboratory and 16 in-situ tests on four different commercially available epoxy based coatings. El-Hawary et al. (1998) conducted compression, tension, flexure, and shear bond tests on concrete specimens repaired by epoxies to study the effect of variables such as types of cement, types of epoxy, duration of exposure to seawater, and the effect of temperature on the strength of epoxy-repaired concrete.

Numerical simulation of repaired concrete can help in choosing an appropriate rehabilitation method and prediction of behavior for the repaired structure. Numerical simulations of epoxy repaired concrete are limited. However, abundant literature has been found on concrete reinforced by other non-metal synthetic materials. Arduini et al. (1997) did experimental, analytical, and numerical study on externally reinforced concrete beams with fiber reinforced plastics (FRP). In this study, experimental results confirmed the possibility of strengthening beams using FRP. However, brittle unexpected failure mechanisms in FRP beams also need to be considered for reinforced beams. An

analytical model is also presented in which the mechanical properties of constituent materials and the characteristics of the interface concrete-FRP are taken into account, and it is supported by numerical simulation. Kachlakev et al. (2001) published a report using the ANSYS program to simulate behavior of four full size beams reinforced with FRP and compared the results to actual load tests. In this simulation, perfect bonding between FRP elements and concrete was assumed. Comparison of the test data and finite element analysis showed good agreement for load deflection and load strain curves and the crack patterns at the final loads. Hu et al. (2004) compared the results of nonlinear finite element analysis of reinforced concrete beams strengthened by fiber-reinforced plastics to laboratory test results and did some parameter studies. In their simulation the reinforcing layer is attached to the concrete beam. Nour et al. (2007) used ABAQUS subroutine to create a constitutive model for concrete and did simulations for concrete structures reinforced with internal and external FRP. In their study a portable constitutive concrete model was proposed that can correctly simulate different kind of composite reinforcements and its reliability was confirmed by the means of several tests. A surface to surface contact interaction was used for simulation of the composite beams.

In order to understand behavior of epoxy-coated concrete, laboratory experiments were performed on epoxy-coated concrete specimens under three load configurations: uniaxial compression, three-point bending and three-edge bearing. The specimens used were concrete cylinders, beams, and pipes which included both epoxy-coated and uncoated ones for comparison. Finite element models of beams and pipes were created using ABAQUS to simulate the epoxy-coated specimens under the studied load configurations. The models were calibrated with laboratory results and a parametric study followed on the effect of interface interaction between concrete and epoxy on the load-deformation curve.

2.2 Experimental Program

A comprehensive laboratory testing program was conducted at the laboratory of the University of Texas at Arlington's Center for Underground Infrastructure Research and Education (CUIRE). Preliminary tests determined the flexural strength of concrete beams as per ASTM C293 and the compressive strength of concrete cylinders per ASTM C39. All the tests were conducted on concrete with design strength of 34.5 MPa and, in both cases, epoxy-coated and uncoated beams and cylinders were used. A total of 5 concrete beams and 17 concrete cylinders were sent to participating companies who applied epoxy using their standard procedure. Cylinders were lined evenly on their whole circumferential surface, and the beams were coated on bottom side that was under tension during loading.

Manufacturers of the epoxy provided the basic mechanical properties of their products. Table 2-1 shows the mechanical properties of the epoxy used in the test provided by two different manufacturers. The epoxy used in this study's test was an ultra-high build epoxy coating formulated with high mechanical strength and resistance to environmental effects.

Table 2-1 Material properties of the epoxy coatings

	Compressive ASTM D695		Flexural ASTM D790		Tensile ASTM D638		Adhesion ASTM D4541	
	Strength (kPa)	E (MPa)	Strength (kPa)	E (MPa)	Strength (kPa)	E (MPa)	Strength (kPa)	Failure mode
EPX1	124,890	2,208	93,840	4,858	57,822	5,023	7,231	100% Concrete
EPX2	72,450	1,932	62,928	759	48,990	649	-	100% Concrete

Pull-off strength or bond testing (ASTM D4541, 2014; ASTM D7234) was also used to measure the adhesion strength between a coating (e.g., epoxy) and a substrate (concrete). The test method requires a dolly (pull stub), which is bonded to the surface of the system. A load is applied to the dolly until failure occurs and the maximum tensile stress is measured. The epoxy materials have excellent bond to concrete and other surfaces as demonstrated in Table 2-1, the failure occurs in concrete in the adhesion test.

Flexural strength of a beam is defined as its ability to withstand bending failure. Standard concrete beams of 15.2 cm × 15.2 cm × 50.8 cm are recommended by ASTM C293. Since flexural tests are sensitive to specimen preparation, handling, and curing procedure, and standard beam specimens were considered heavy and requiring longer curing time, the specimen size was reduced to 7.6 cm × 7.6 cm × 28 cm to facilitate the handling and transportation process. Concrete beams were coated with epoxy at the bottom tension side for flexural strength test as shown in Figure 2-1. In the flexural strength test, the concrete beam was loaded with three-point loading and failed due to development of tension cracks. Therefore, the tension behavior of concrete is the most important property that determines the structural capacity of the concrete beam. For the coated concrete beam, the structural capacity increased greatly compared to the bare

concrete beam as shown in Table 2-1. The increase of structural capacity (strength) was due to the reinforcement effect of epoxy on concrete, which resulted in stiffening of the tension-stiffening curve. An extensive parameter study was performed to evaluate the load-deflection curve in response to each tension-stiffening parameter. The flexural behavior of concrete for coated and uncoated beams was back-calculated from measured laboratory test. The ultimate strain for bare concrete and reinforced concrete was assumed to be close to the failure strain of the epoxy, which is 0.016. The mechanical properties shown in Table 2-1 were considered in modeling epoxy materials. A bilinear material model was selected with elasticity modulus of 5,019 MPa, a yield stress of 31 MPa, and an ultimate strength of 58 MPa.

Figure 2-1 A typical coated beam specimen (image by Alimohammad Entezarmahdi)

Compressive strength tests on both coated and uncoated 10 cm x 20 cm cylindrical concrete samples were performed. Epoxy coating was applied in the form of a wrap to the outer side of each concrete cylinder. Summary of the test results for coated and uncoated concrete cylinders and beams are presented in Table 2-2.

Table 2-2 Summary of Test Results of Uncoated and Coated Concrete Samples

Test type	Uncoated Specimen (average of 3)	Coated Specimen (average of 5)
Compression Strength –Cylinder (kPa)	35,073	38,868
Flexural Strength -Beam (kPa)	6,320	11,433

2.3 Three-edge Bearing Test of Precast Reinforced Circular Concrete Pipes

A three-edge bearing test was performed per ASTM C497 to evaluate the behavior of the lined and unlined concrete pipes. The main purpose of this test was to determine the effect of applying epoxy liners on the ultimate strength of lined precast circular pipes. An unlined pipe was also tested to provide a comparison base. The concrete pipes were dry precast pipes manufactured according to ASTM C76 which are typically used for storm sewer and roadway drainage applications. The pipes have an inside diameter of 61 cm with 7.6 cm thickness and 1.2 m length. A total number of 17 pipes including one unlined pipe were tested. The three-edge bearing method was used for loading the pipes. In this method, a pipe was supported on a lower bearing of two parallel longitudinal strips, and the load was applied through an upper bearing. Twenty-eight days or more after the pipe was casted, participating manufacturers of different liners came to the site of the pipe manufacturer (Forterra Pipe & Precast, Grand Prairie, Texas) to apply linings on the pipe's inner surface following their routine standard operation to represent the field operation procedure. Also one day before the lining process, strain gages were installed by the UTA research team. The strain gages were installed on selected pipes, as shown in Figure 2-2 (a), at four critical locations where maximum strains are anticipated. Strain gauges (model PFL-30-11 from Vishay, Malvern, Pennsylvania) were selected and installed on the concrete surface using a bonding material supplied by Vishay. The concrete surface was processed to provide smooth and

clean surface for bonding application. The strain gauges were attached to the surface and remained until the bonding materials were completely hardened, after which the lining process was initiated. After the lining process was completed, displacement transducers DP-1000 E from Tokyo Sekki Kenkyujo (Shingawa-ku, Tokyo, Japan) were attached to the top and bottom of the pipe for measuring pipe deformation in a vertical diameter direction during loading. Figure 2-2 (b) shows an example pipe with liner and instrumentation ready for three edge bearing load test.

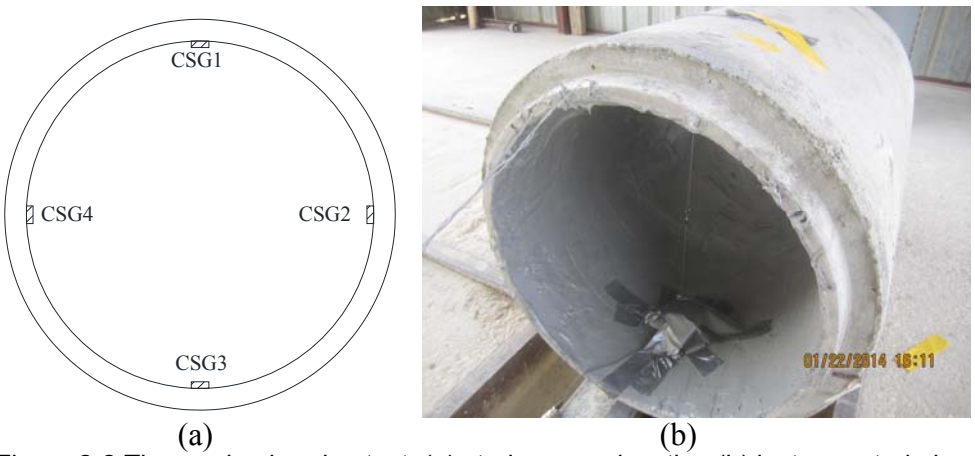

(a) (b)

Figure 2-2 Three-edge bearing test: (a) strain gauge location (b) instrumented pipe sample (image by Alimohammad Entezarmahdi)

A hydraulic jack was used to apply load with the maximum loading rate of 16 kN/min. Two load cells were installed to record applied load during the loading process. Data acquisition was performed using the strain gauges and displacement transducer (Sekki Kenkyujo, Tokyo, Japan). According to the ASTM standard, the maximum load supported by pipe is reported as ultimate strength. The D-load strength was calculated by dividing the maximum strength by the length of the pipe and the inside diameter of the pipe (ASTM C497). Figure 2-3 shows pipe crushing tests conducted on unlined concrete pipe and lined pipe. Figure 2-3 shows distinct cracks in both pipes after maximum load was applied. The crack pattern of liners varied according to the liner materials. Other

specimens had no obvious cracks in the liner. Results from the pipe crushing test indicate that the peak D-load strength of unlined concrete pipe is 82.7 kPa and the average D-load strength for the pipes lined with epoxy is 172 kPa.

(a) (b)

Figure 2-3 Pipes after three-edge bearing test: (a) example unlined pipe; (b) example lined pipe (image by Alimohammad Entezarmahdi)

Strain gauges CSG1 and CSG3 are located at the top and bottom of the pipe and strain gauges CSG2 and CSG4 are located on the two sides. Results obtained from experiments on pipe lined by EPX2 did not show a reasonable trend probably due to false strain gage readings; hence, EPX2 results are not shown in Figure 2-4. In the case of EPX3, results from CSG2 were reasonable. CSG1 readings for EPX3 showed significantly less strain compared to other readings which might be caused by poor bonding between the strain gage and concrete surface. The displacement transducer was only installed for tests on EPX1 (Raven 405, Raven Lining System, Broken Arrow, Oklahoma) and EPX2 (Permaform, AP/M Permaform, Johnston, Iowa). The load versus deformation is plotted in Figure 2-5.

According to the obtained data presented in Figure 2-5, EPX1 shows less deformation and a higher peak load. By comparing the epoxy properties shown in Table 2-1, epoxy used in EPX1 has a much higher flexural strength compared to epoxy used in EPX2. Therefore, pipe EPX1 has much higher structural capacity and less

deformation, although EPX2 has a thicker liner. Figure 2-5 also shows data noise, which is caused by wind vibration of the transducer cord.

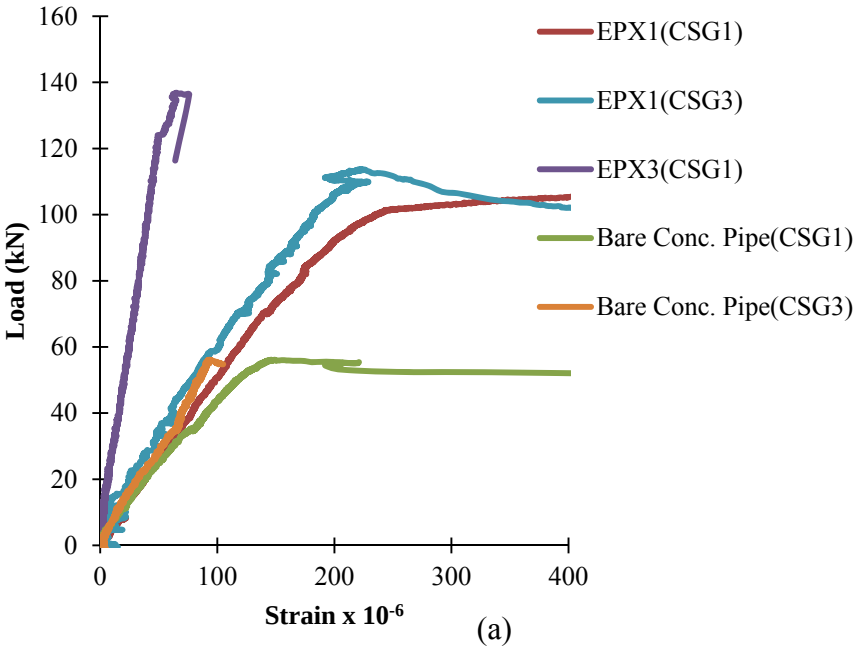

Figure 2-4 Measured load-strain curves for both lined and bare concrete pipes: (a) strain gages at location 1 and 3; (b) strain gages at location 2 and 4

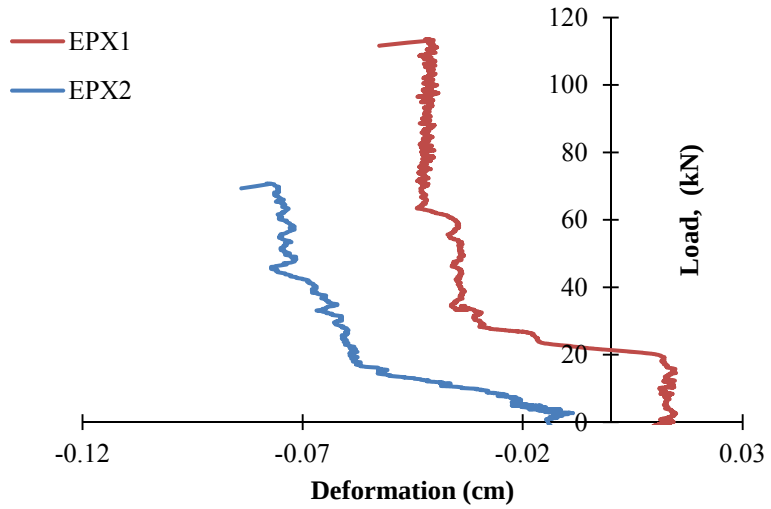

Figure 2-5 Load deformation curves for lined pipes from D-load test

2.4 Finite Element Modeling

The multipurpose finite element (FE) software suite ABAQUS was selected to simulate the behavior of epoxy-coated and uncoated concrete specimen under the above mentioned load configurations. Simulation of a flexural strength test of a coated beam was validated with the beam test results. The calibrated material models were then used in the pipe simulation. For each case, simulations were performed on both lined pipe and uncoated concrete beams to study the effect of epoxy coating on concrete strength.

2.4.1 Material Models

Concrete damaged plasticity model (ABAQUS analysis user's manual), available in the ABAQUS material library, was used to simulate concrete behavior under compression and tension. According to the ABAQUS v 6.12, concrete damaged plasticity constitutive theory aims to capture the effects of irreversible damage associated with failure mechanisms that occur in concrete and other quasi-brittle materials under fairly low confining pressures. The plastic-damage model in ABAQUS is based on models proposed by Lubliner et al. (1989) and by Lee and Fenves (1998). The epoxy was modeled as perfect elastic and plastic material. The input parameters for concrete

presented in Table 2-3 are determined from laboratory tests on uncoated concrete cylinders and bare concrete beams. For parameters that cannot be directly determined from these tests, values were estimated from literature.

2.4.2 Tension Stiffening Curve

As mentioned before crack propagation in concrete is modeled with a tension stiffening curve, which allows definition of the strain-softening behavior for cracked concrete. This behavior also allows the effects of the reinforcement interaction with concrete to be simulated in a simple manner. Tension stiffening is required in the concrete damaged plasticity model. Tension stiffening can be specified by means of a stress and cracking strain relation or by applying a fracture energy cracking criterion (ABAQUS Theory Manual). By using the results from flexural strength tests on coated and uncoated concrete beams, tension stiffening curves were established for both beams through optimization as shown in Figure 2-6.

Table 2-3 Concrete Material Property

Modulus of Elasticity (GPa)		30
Poisson Ratio		0.2
Density (kg/m^3)		2400
Plasticity	Dilation Angle (°)	38
	Eccentricity	0.1
	f_{b0}/f_{c0}	1.16
	K	0.667
	Viscosity Parameter (s)	10^{-7}

Note: fb0=fc0 = ratio of initial equibiaxial compressive yield stress to initial uniaxial compressive yield stress (the default value is 1.16); K = ratio of the second stress invariant on the tensile meridian, to that on the compressive meridian, at initial yield for any given value of the pressure invariant p such that the maximum principal stress is negative.

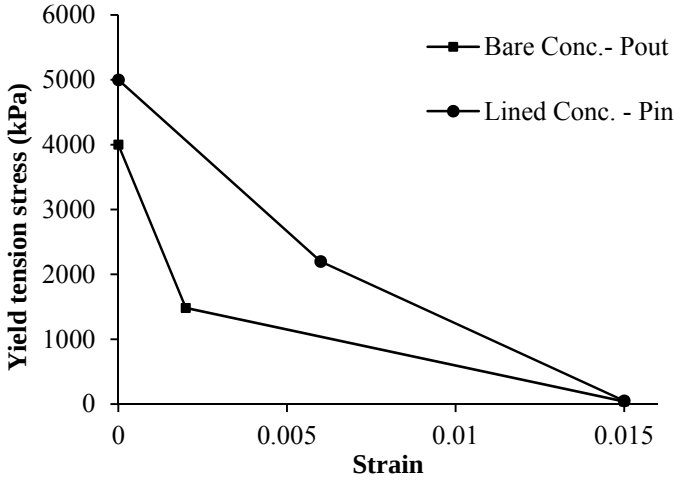

Figure 2-6 Tension stiffening curves for coated and uncoated concrete

2.4.3 Interaction Models

Two contact surface interaction models were used - one with a friction surface and the other with a cohesive surface - to simulate the interaction between the epoxy and the concrete substrate in coated beams and lined pipes. For the coated beam simulation, a surface-to-surface contact with frictional behavior was used as no surface separation was expected. The tangential property of the contact was considered as “penalty” with a friction coefficient of 0.5, and the normal property was chosen as “hard contact” without separation.

The hard contact model cannot simulate adhesion when separation of contact surface occurs. Therefore, a surface to surface contact with cohesive behavior was also used to simulate adhesion between lining and concrete substrate, and the results were compared to select the best interaction model for the simulation. Surface-based cohesive behavior provides a simplified way to model cohesive connections with negligibly small interface thicknesses using the traction-separation constitutive model. The formulae and laws that govern surface-based cohesive behavior are: linear elastic traction-separation,

damage initiation criteria and damage evolution laws (ABAQUS). Figure 2-7 shows a typical traction-separation response with a failure mechanism.

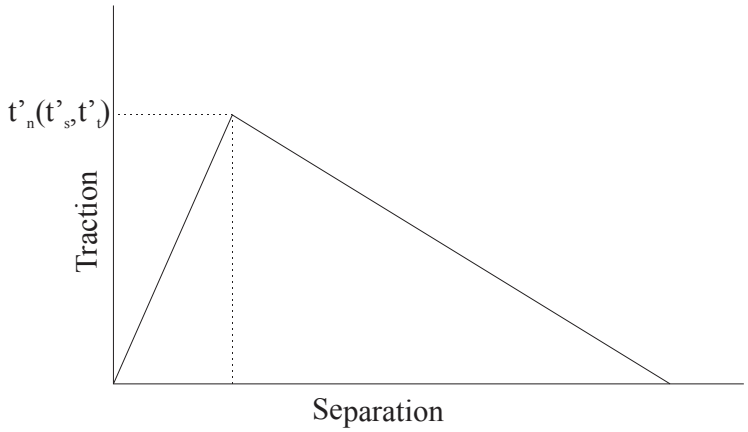

Figure 2-7 Typical traction-separation response **(**ABAQUS**)**

In this simulation the cohesive behavior was inferred from bond testing results provided by the manufacturer. The stiffness of the underlying material was considered 17.5 kN/cm in all directions and a set of bonded nodes was defined on the exterior edge of the epoxy layer to which the cohesive interaction was applied. For damage initiation the maximum stress was set to 2200 kPa in all directions and damage evolution with a ratio of 2 for total displacement to the plastic displacement was used.

2.4.4 Flexural Strength Test of Beams

A 3D beam with eight-node linear brick elements was created in ABAQUS to model flexural strength test of the concrete beam as shown in Figure 2-8. A model concrete beam of 7.6 cm × 7.6 cm × 28 cm was created and three rigid strips were tied to the beam, two at the bottom (representing the supports) for applying boundary conditions and one on top (representing the loading nose) for applying a displacement boundary condition to simulate the loading process. The strips were used to avoid stress concentration. The beam was restrained from movement in vertical (y) direction at the

bottom and constrained in x and z direction on top. All the boundary conditions were applied to the rigid strips. For the coated beam model, the coating was simulated by adding a 3 mm. thick epoxy layer beneath the concrete beam. The interaction between the concrete beam and the epoxy layer was simulated using the hard surface contact model available in ABAQUS. A comparison of simulation results between uncoated concrete beams and coated concrete beams validated the contact model for the epoxy and concrete interaction. The flexural strength test results for uncoated concrete beams, and the selected epoxy-coated concrete beams are shown in Table 2-2. The average values were used as the laboratory testing values for comparison with ABAQUS simulations. No deformation measurement was available from laboratory testing of beams; therefore, the calibration of ABAQUS simulation is mainly based on the measured strength.

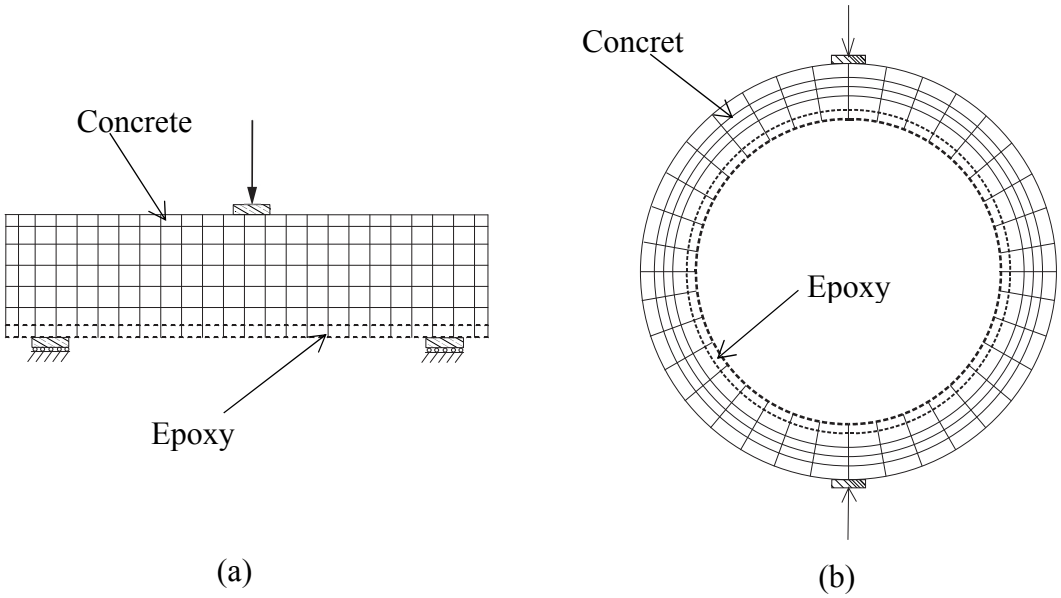

Figure 2-8 Conceptual models of ABAQUS beam and pipe simulations: (a) Case I- Flexural Strength; (b) Case II- Pipe Crushing

2.5 Three-edge Bearing Test of Concrete Pipes

FEM simulation of the pipe crushing test was performed to study the lining reinforcement effect under three-edge loading condition as shown in Figure 2-8. A concrete pipe with a 61 cm. inside diameter and 7.6 cm. wall thickness was modeled using 4 node bilinear plane stress quadrilateral elements (CPS4R) in ABAQUS. The 2D model was generated using plane stress shell elements to account for its free end boundary condition. Both lined and unlined concrete pipe were simulated. For the lined pipe, a 6 mm layer of epoxy was applied to the inside of the concrete pipe.

The pipe was restricted from moving in a vertical direction at the bottom and from moving in a horizontal direction on top. The displacement controlled loading was applied at the top of the pipe. In order to avoid stress concentration, the boundary conditions and the load were applied by using rigid plates on the top and bottom of the pipe. The rigid plates were tied to the pipe.

In the case of unlined concrete pipe, uniform concrete material property was assigned to the entire pipe cross section and a 0.5 cm. deflection was applied to the rigid plate on top of the pipe. The tension stiffening curve used for this simulation was the same as the curve obtained from the bare concrete beam test. The other case was simulated by using the same concrete pipe and adding a layer of epoxy inside of it. Two different types of interactions were used to simulate the interaction between the concrete and the lining; one was modeled by means of cohesive interaction and the other by frictional interaction. Two different tension behaviors were assigned to the concrete for simulation of lined concrete pipe. The concrete outside of the center line of the concrete pipe wall had no reinforcement (pure concrete); the concrete inside the center line had the same tension stiffening curve as that obtained for lined concrete beam simulation. The tension stiffening curve for the reinforced concrete is shown in Figure 2-6. P_{out} is the

tension stiffening curve for concrete on the outside of the pipe wall centerline. P_{in} is the tension stiffening curve with lining reinforcement inside of the pipe wall centerline. As mentioned before the curves were obtained from the results of concrete beam tests.

2.6 Numerical Results and Validation

2.6.1 Flexural Strength Test of Beam

Figure 2-9 (a) presents the location of the crack in the coated concrete beam, as predicted by ABAQUS. Compared to the actual test [Figure 2-9 (b)], it can be seen that the simulation can accurately predict the crack propagation in the beam.

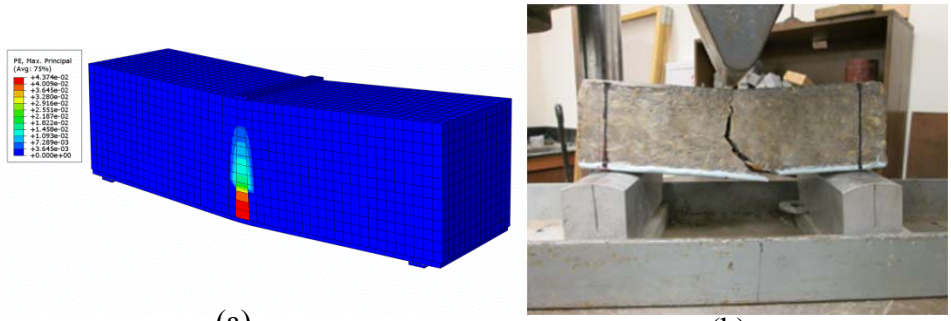

(a) (b)

Figure 2-9 (a) Crack in FEM simulation of the coated concrete beam; (b) test photo of the simulated coated concrete beam (image by Alimohammad Entezarmahdi)

As shown in Figure 2-10 the peak load obtained from simulation was 8 kN with a deflection of 0.04 mm which is in good agreement with the average peak load from laboratory tests on uncoated concrete equal to 8.2 kN. For coated concrete beams, the peak load from laboratory test was 12.9 kN, and the peak load from the simulation was 13 kN with a deflection of 0.12 mm. This comparison indicates accuracy of the simulation. The simulations also indicate that the frictional interaction with concrete tension stiffening curve can simulate the lined concrete beam properly.

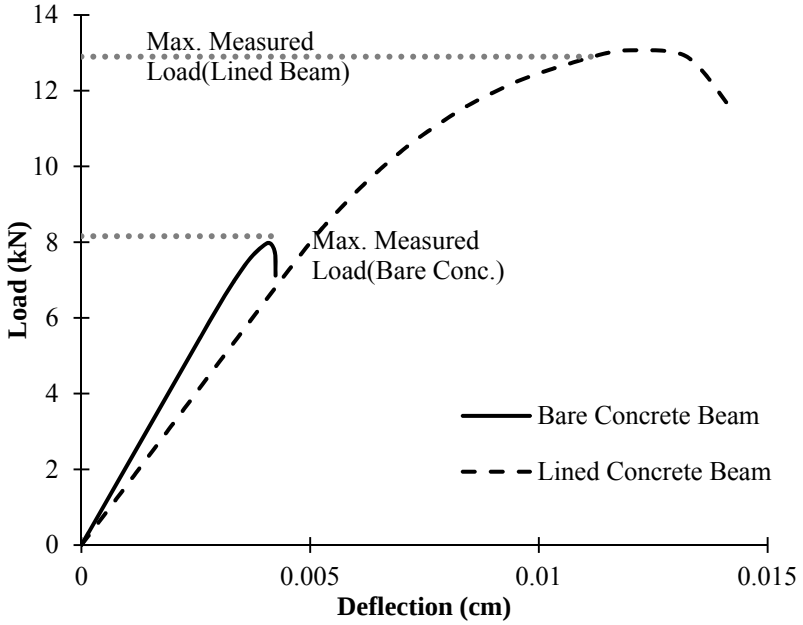

Figure 2-10 Load deflection curve from ABAQUS simulation for bare and lined concrete

2.6.2 Three-edge Bearing Test of Pipe

The simulated failure pattern of bare concrete pipe is shown in Figure 2-11(a) compared to the actual failure pattern shown in the tested pipe's photograph. The predicted cracks, the bright areas in the plastic strain contour, agree with the actual cracks [Figure 2-11 (b)]. Load-deformation curves obtained from the simulations in this case are shown in Figure 2-12 which indicates a peak load of 69 kN at 0.35 mm deformation for unlined concrete pipe. Figure 2-12 compares the load-deflection curve of the pipe for lined and unlined concrete pipe with two different types of interaction models. Comparison of load deflection curves for the simulations shows that using an epoxy layer with a cohesive interaction behavior increases the load capacity of the pipe.

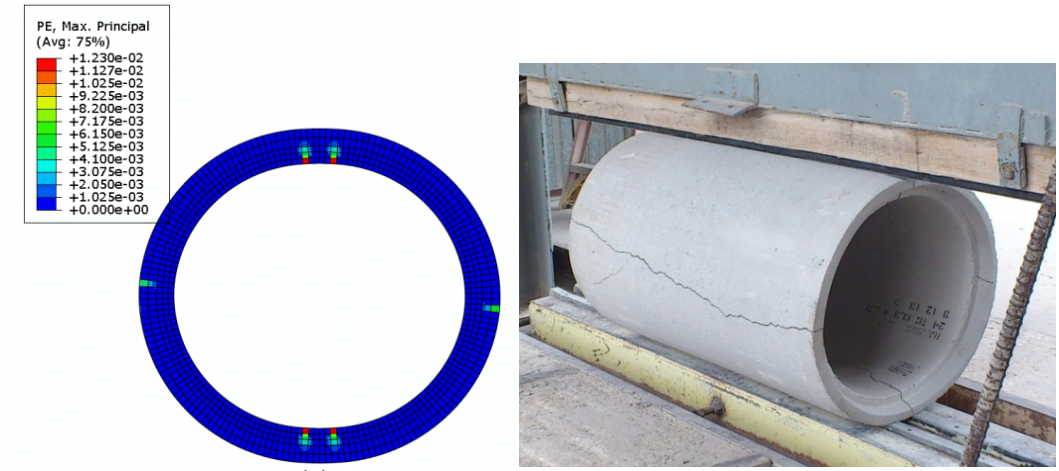

Figure 2-11 (a) Cracks in FEM simulation of the unlined concrete pipe; (b) photo of unlined concrete pipe after thee-edge bearing test (image by Alimohammad Entezarmahdi)

As previously mentioned, test results for load deformation curves were available only for EPX1 and EPX2. The results from the simulation and test results are compared in Figure 2-13. The results from the simulation for different lining materials are close to each other, and they are in good agreement with test results of EPX1.

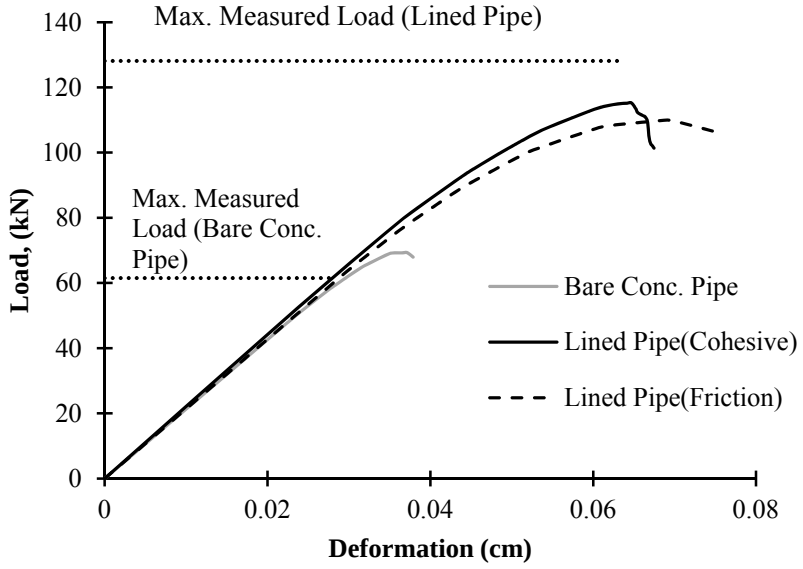

Figure 2-12 Load deformation curve of unlined and lined concrete pipe

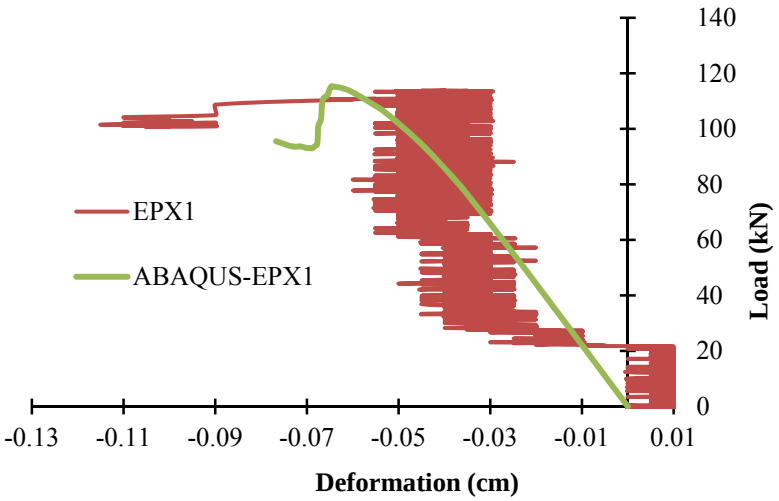

Figure 2-13 Load deformation curve of lined concrete pipe

Figure 2-14 compares the results obtained from ABAQUS simulation to the test results for EPX1. As mentioned before, the strain gauges were installed inside of the pipes before applying the coating. Since there is the possibility that the data obtained from the strain gauges refers to the strain of the epoxy lining, strain output for the epoxy is also presented in the graphs to compare the results with test data.

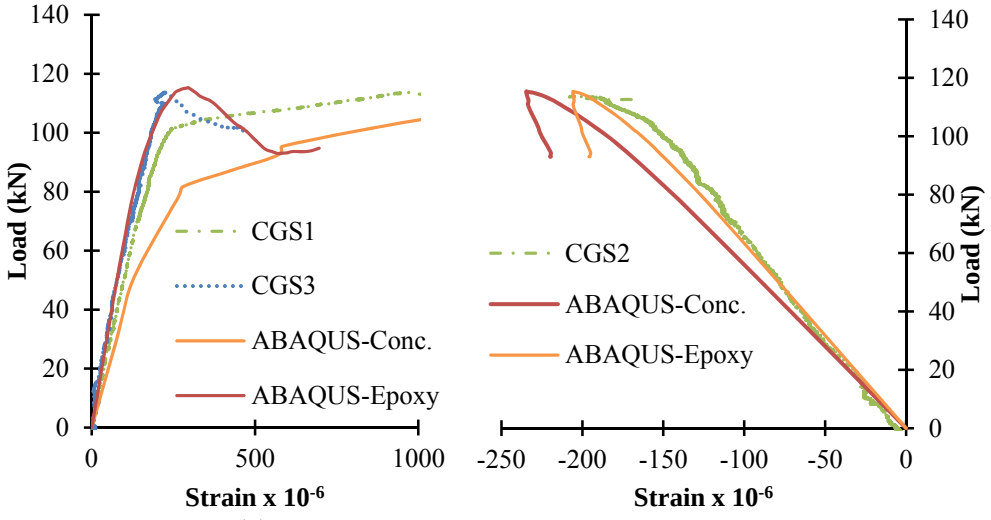

Figure 2-14 Comparison of the measured strain with ABAQUS simulation for the pipe lined with EPX1: (a) strain at location 1 and 3; (b) strain at location 2

As shown in the graph the results from simulation and the test are in good agreement. The linear part for all of the data matches, and the peak load from the simulation is almost the same as the peak load from the test. Comparing the results obtained from CGS3 strain gauge with the result of strain induced in the epoxy during the simulation as shown in the Figure 2-14, shows that the two curves are laying on each other which can be indicating that the readings from the CGS3 strain gauge refers to the strain induced in the coating. Figure 2-15 compares the results obtained from the pipe crushing test on unlined concrete pipe and ABAQUS simulation.

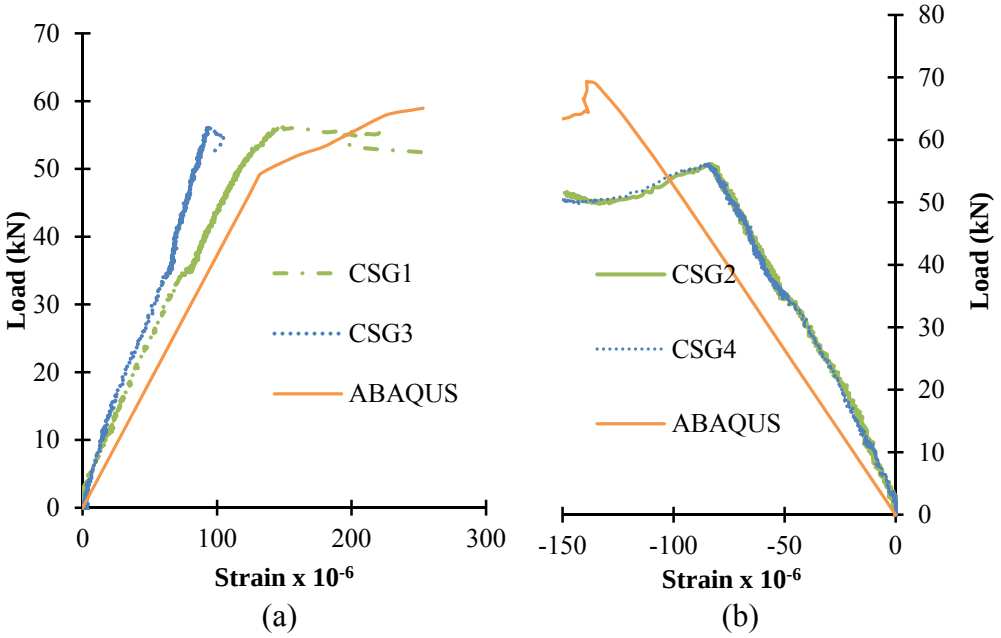

Figure 2-15 Comparison of the measured strain with ABAQUS simulation for the unlined pipe: (a) strain at location 1 and 3; (b) strain at location 2 and 4

The results indicate that in the linear part of the graph, simulation is predicting the behavior of the unlined concrete pipe acceptably but the peak load obtained from the simulation is larger than the test results.

2.7 Parametric Study

After verification of the model using test results, a parametric analysis was performed to better understand the effect interaction model between the concrete and epoxy lining on the strength of beams and pipes.

In beam simulation two different interaction models were studied. In the first one (as presented previously), the interaction between the beam and the lining was simulated using frictional behavior. For this approach three different friction coefficients were assigned and the results for load deflection curves were obtained and compared as shown in Figure 2-16.

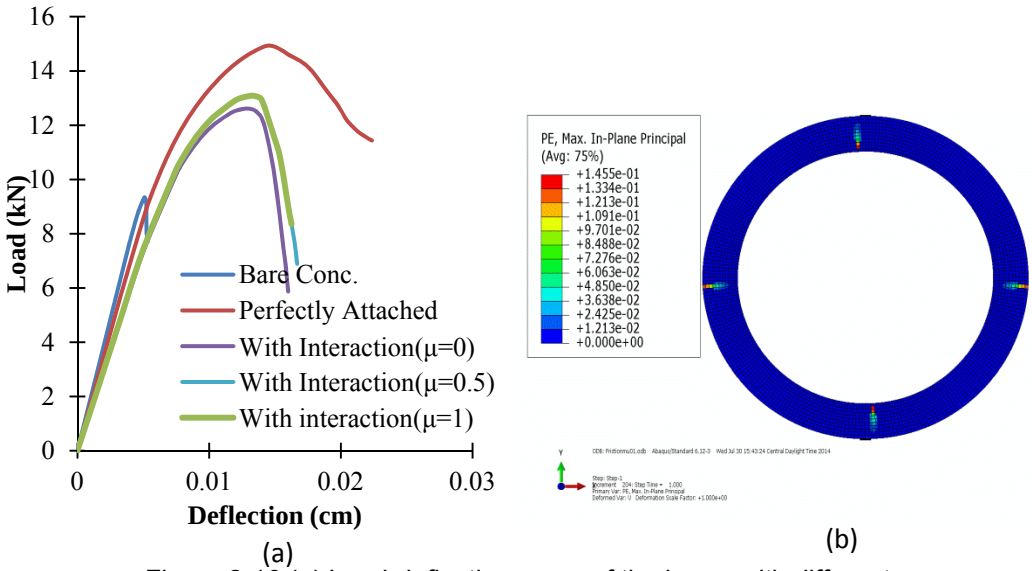

(a) (b)

Figure 2-16 (a) Load-deflection curve of the beam with different interactions (b) Crack formation in the lined concrete pipe

In the second model the simulation was performed by considering a perfect attachment between the concrete and its lining. In this case the beam and lining were modeled as one part and different material properties were assigned to the concrete and the lining by using partitioning. The load deflection curve for this case was is also presented in Figure 2-16. The curves show that using frictional behavior between the

concrete beam and lining with three different friction coefficients (Model 1) does not change the peak load that can be carried by the lined beam. Comparison of the results with the case of tie between the lining and concrete (Model 2) showed an increase of about 11% in the peak load.

The same parametric study was performed for the pipe crushing test. In one case the lining and the concrete were considered as one part and partitioning was used to assign different material properties to the concrete and the lining, which is referred to as perfect attachment. In the two other cases two different interaction models were used, frictional behavior and cohesive surface behavior. Comparison of the load deflection curves is presented in Figure 2-17. The results show that the peak load considering perfect attachment between the pipe and lining is higher than the other approaches.

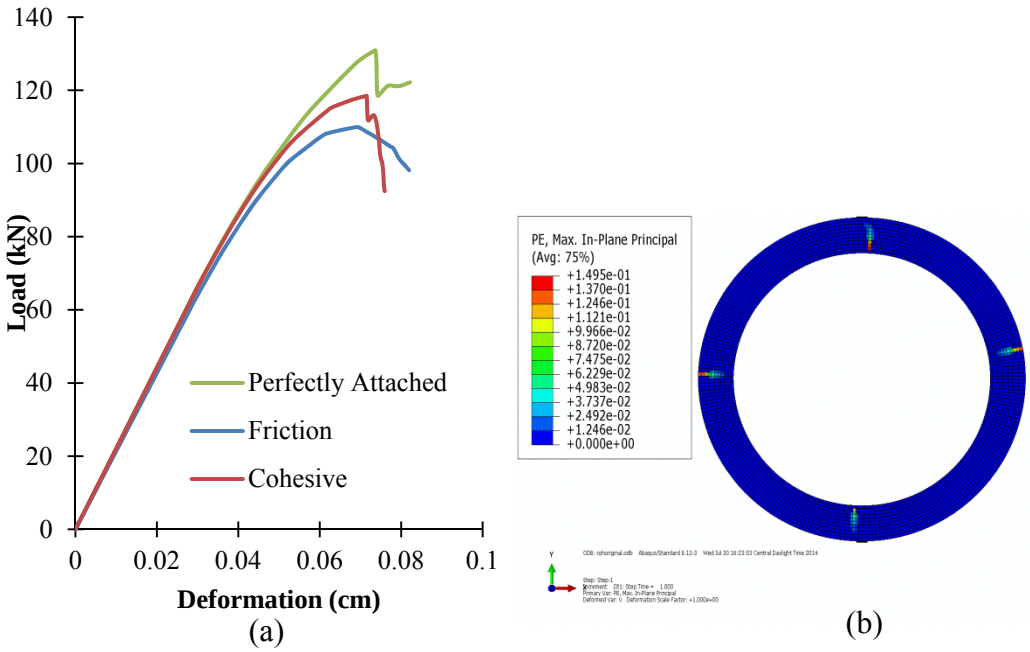

Figure 2-17 (a) Load-deflection curve of the pipe with different interaction simulation approaches (b) Crack formation in lined concrete pipe with cohesive interaction

Different friction coefficients have also been used for frictional interaction and the results did not show any significant change in the load deflection curve.

2.8 Conclusions

Laboratory tests were performed to study the lining effect on improving load bearing capacity of beams and pipes. The test results on concrete beams showed that the epoxy application can noticeably improve the flexural strength of a concrete beam. A finite element model was first developed with epoxy coated concrete beam simulations. Concrete and epoxy material properties and the interaction property between the epoxy and concrete were calibrated through the simulated epoxy-coated beam. The calibrated model was used to simulate three-edge crushing test of pipe. The simulation results for pipe was also compared to the pipe crushing test results and show that the epoxy lining can increase the pipe structural capacity for the pipe crushing , and this increase was affected by the lining adhesion and tension reinforcement effect. The simulations indicate that the structural capacity of epoxy coated or epoxy lined concrete structures was highly dependent on the loading conditions. Structures controlled by tension failure can benefit significantly when lined with tension resistant coatings such as epoxy. The adhesion of coating can also affect the structural capacity when linings are subjected to tension stress normal to the contact surface.

Finally the calibrated models were used to perform parametric studies on the effect of an interaction model. The results show that with mesh tie interaction between the lining and concrete the peak load increases for beam and pipe simulation while using different friction coefficients in both cases did not affect the peak load significantly.

Acknowledgment

This work is partially supported by the Water Environmental Research Foundation (WERF) grant, project number INFR1R12. The financial support is acknowledged.

References

ABAQUS version 6.12 [Computer software]. Dassault Systèmes SIMULIA, Providence, RI.

ANSYS version 5.5 [Computer software]. ANSYS, Canonburg, PA.

Arduini, M., Tommaso, A. D., and Nanni, A. (1997). “Brittle failure in FRP plate and sheet bonded beams.” ACI Struct. J., 94(4).

ASTM. (2010a). “Standard test method for flexural strength of concrete.” ASTM C293, West Conshohoken, PA.

ASTM. (2010b). “Standard test methods for flexural properties of unreinforced and reinforced plastics and electrical insulating materials.” ASTM D790, West Conshohoken, PA.

ASTM. (2012). “Standard test method for pull-off adhesion strength of coatings on concrete using portable pull-off adhesion testers.” ASTM D7234, West Conshohoken, PA.

ASTM. (2014a). “Standard test method for concrete pipe, manhole sections, or tile.” ASTM C497, West Conshohoken, PA.

ASTM. (2014b). “Standard test method for pull-off strength of coatings using portable adhesion testers.” ASTM D4541, West Conshohoken, PA.

ASTM. (2014c). “Standard test method for reinforced concrete culvert, storm drain and sewer pipe.” ASTM C76, West Conshohoken, PA.

ASTM. (2014d). “Standard test method for tensile properties of plastic.” ASTM D638, West Conshohoken, PA.

ASTM. (2015a). “Standard test method for compressive properties of rigid plastics.” ASTM D695, West Conshohoken, PA.

ASTM. (2015b). “Standard test method for compressive strength of cylindrical concrete specimens.” ASTM C39, West Conshohoken, PA.

El-Hawary, M., Al-Khaiat, H., and Fereig, S. (1998). “Effect of sea water on epoxy-repaired concrete.” Cem. Concr. Compos., 20 (1), 41–52.

Hu, H. T., Lin, F. M., and Jan, Y. Y. (2004). “Nonlinear finite element analysis of reinforced concrete beams strengthened by fiber-reinforced plastic.” Compos. Struct., 63, 271–281.

Kachlakev, D., Miller, T., Yim, S., Chansawat, K., and Potisuk, T. (2001). “Finite element modeling of concrete structures strengthened with FRP laminates.” Final Rep. FHWA-OR-RD-01-17.

Lee, J., and Fenves, G. L. (1989). “Plastic-damage model for cyclic loading of concrete structures.” J. Eng. Mech., 10.1061/(ASCE)0733-9399 (1998)124:8(892), 892–900.

Liu, J., and Vipulanandan, C. (2005). “Tensile bonding strength of epoxy coatings to concrete substrate.” Cem. Concr. Res., 35 (7), 1412–1419.

Lubliner, J., Oliver, J., Oller, S., and O˜nate, E. (1989). “A plastic-damage model for concrete.” Int. J. Solids Struct., 25(3), 229–326.

Nour, A., Massicotte, B., Yildiz, E., and Koval, V. (2007). “Finite element modeling of concrete structures reinforced with internal and external fibrereinforced polymer.” Can. J. Civ. Eng., 34, 340–354.

Saxena, S. K. (2014). “Epoxy resin-its application in structural repairs.” Government of India, Ministry of railways, Gwalior, India.

Chapter 3

Structural Behavior of Concrete Pipe With Spray-On Cured In Place Lining

Underground structures are widely used throughout the world and having a good understanding of their behavior can help establish more efficient use and design. Concrete pipes are one of the most common infrastructures and due to their exposure to different environmental conditions, they are subject to deterioration. One rehabilitation method is spray-on cured-in-place lining, which has become more popular due to its simplicity and cost efficiency. Rehabilitated concrete pipes are referred to as composite pipes and have a different structural behavior. Behavior of composite concrete pipes under D-load and coated concrete beams under third point bending tests were studied in this paper. Results from beam tests are used to obtain a valid tension softening curve for concrete simulation. The results obtained from three-edge bearing tests on concrete pipes with different types of polymeric linings are presented and a finite element model is generated to study the behavior of the pipes under D-load. The parametric studies show that increasing the thickness of lining in the deteriorated concrete pipe, which is represented by decreasing Young's modulus of concrete, improves load bearing capacity of the pipe.

3.1 Introduction

Underground infrastructures such as pipelines, are widely used throughout the world. These embedded structures play an important role in the development of cities. Regarding special environment, surrounding underground structures compared to other structures have a high risk of deterioration. Deterioration is loss of structural capacity with time as a result of external factors such as overloading, earthquake and cyclones or

material weakening in an aggressive environment such as sulfate attack and chloride ion penetration (1). Pipeline failure can cause potential of flooding neighborhoods and residences, traffic disruption and pollution of underground water resources and it can result in costly consequences (2). To avoid pipeline failure, an effective treatment must be adopted to stop the collapse process in its first stage which is pipe cracking caused by poor construction, practice or subsequent overloading or disturbance (3). Due to difficulty in access and maintenance of these structures it is important to find a practical and efficient way to confront degradation of pipes.

Pipes are manufactured with different materials such as steel, PVC, concrete, etc. Concrete pipe has a long history of excellent performance as a durable product for storm water drainage and sewer applications in different sizes all over the world. As mentioned above, like any other structure, concrete pipe may experience structural decay during its service, which must be addressed appropriately. There are several ways to deal with concrete pipe deterioration, such as replacement, chemical grouting, pipe linings, coatings and robotic rehabilitation (4).

Spray-on lining is the oldest method of pipeline rehabilitation. In this method, a polymeric lining like epoxy and polyurethane or cement mortar is sprayed inside of the deteriorated pipe to stop internal corrosion, restore hydraulic capacity, and eliminate water quality deterioration arising from iron or steel corrosion and associated scaling. The ability to achieve one-day return to service, nearly effortless service reconnections, minimal community impacts, and low installation costs are the main attractive features of spray-on lining compared to other rehabilitation methods used for water mains. Uncertainty about structural benefits of these linings has always categorized their application as a “non-structural” rehabilitation method (5).

Structural capacity of spray-on linings was studied by the Water Research Foundation in 2010 (5). In this project, the structural abilities of spray-on linings are examined and the focus is largely on polymeric linings. This research led to the development of new laboratory tests performed on samples of in-situ lined cast iron pipe. Case studies were also developed, which describe how these linings are currently being applied in North America and the United Kingdom (5). Another research project performed by the Water Environment Research Foundation (WERF) in 2015 (6) presents a study of the structural capabilities of no-dig manhole rehabilitation. The results of this project suggest that any type of manhole rehabilitation material can be applied as fully structural; nevertheless, it may be difficult to achieve the thickness required to qualify as fully structural for the spray-applied, cured-in-place type liners (6).

To the best of this author's knowledge, literature on the structural capacity of spray-on linings for concrete pipes is limited. This paper focuses on structural behavior of concrete pipes that are lined with polymeric linings. The results from a set of three-edge bearing tests on bare and lined concrete pipes are carried out as part of the Water Environment Research Foundation (WERF) research program at the University of Texas at Arlington (UTA) and the Center for Underground Infrastructure Research and Education (CUIRE). The tests were carried out on one concrete pipe without lining as a control (for comparison) and 16 concrete pipes with different lining materials. The results obtained from the tests were adopted to generate a finite element model using the multipurpose commercial software, ABAQUS, and to perform a parametric study on behavior of composite concrete pipe.

3.2 Experimental Program

3.2.1 Three-Edge Bearing Test

To study the effect of applying different linings in concrete pipe, a set of 17 three-edge bearing tests per ASTM-C497 (7), was performed by the research group at University of Texas at Arlington (UTA), Center for Underground Infrastructure Research and Education (CUIRE). According to ASTM-C497 (7), 12 different test methods are used in production and acceptance testing of concrete pipes to evaluate the properties provided as pipe specifications. One of the tests is performed to calculate external load crushing strength of the concrete pipe. This strength is measured by the three-edge bearing test method. In this test method, the specimen is tested in a machine designed to apply a crushing force upon the specimen in a plane through the vertical axis extending along the length of specimen. The results from the external load crushing strength test shall be used as a quality control or as a proof of adequacy of design.

In a three-edge bearing test, the specimen is supported on the lower bearing of two parallel longitudinal strips and the load is applied through a substantial and rigid upper bearing. The test specimen is placed on the two lower bearing strips and the upper bearing is aligned in the middle of the lower bearing strips. For non-reinforced concrete pipes the maximum loading rate is 110 kN/linear meter of pipe per minute and after that loading rate is reduced to a maximum uniform rate of one third of the specified design strength of the pipe per minute. The design strength is expressed as a D-load supported by the pipe before a crack having a width of 0.01 inch occurs throughout a continuous length of 1ft or more measured parallel to the longitudinal axis of pipe barrel.

The ultimate strength is the maximum load supported by the pipe. The ultimate strength in pound per linear foot is calculated by dividing the maximum test load applied to the pipe length and the D-load strength in kilonewton per linear meter. The inside diameter or horizontal span shall be either the 0.254 mm crack D-load strength or the

ultimate D-load strength. They are both calculated by dividing the corresponding load to the length and to the inside diameter of the pipe (7).

Precast reinforced concrete pipes with 61 cm inside diameter, 7.6 cm thickness, and 1.2 m length are used for three-edge bearing tests. Concrete pipes are prepared per ASTM-C76 (8) which are typically used for storm sewer application.

Concrete pipes are prepared and lined by each lining manufacturer's certified contractors. After surface preparation of the concrete pipes, four strain gauges (model PFL-30-11 from Vishay, Malvern, Pennsylvania) are installed inside of the selected pipes at top, bottom and on two sides to measure strains induced in the pipe during the test. Strain gauges are installed at critical points where maximum strains are anticipated. **Error! Reference source not found.**(a) illustrates the position and name of each strain gauge. Linings are applied after strain gauge installation. A sample lined concrete pipe is shown in **Error! Reference source not found.**(b).

D-load is applied using a hydraulic jack with a maximum rate of 16 kN/min, and two load cells record the applied load during the loading process. All the tests are performed on the pipe manufacturer site (Forterra Pipe & Precast, Grand Prairie, Texas).

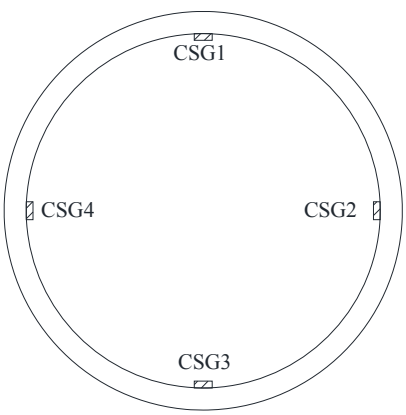

(a) (b)

Figure 3-1. Three-edge bearing test: (a) strain gauge locations and (b) lined pipe sample (photo by Alimohammad Entezarmahdi)

Test results from six different linings and unlined concrete pipe indicate that for all of the cases using the lining, the ultimate D-load increases according to results obtained from the three-edge bearing test. **Error! Reference source not found.** presents load versus strain curves obtained from the tests.

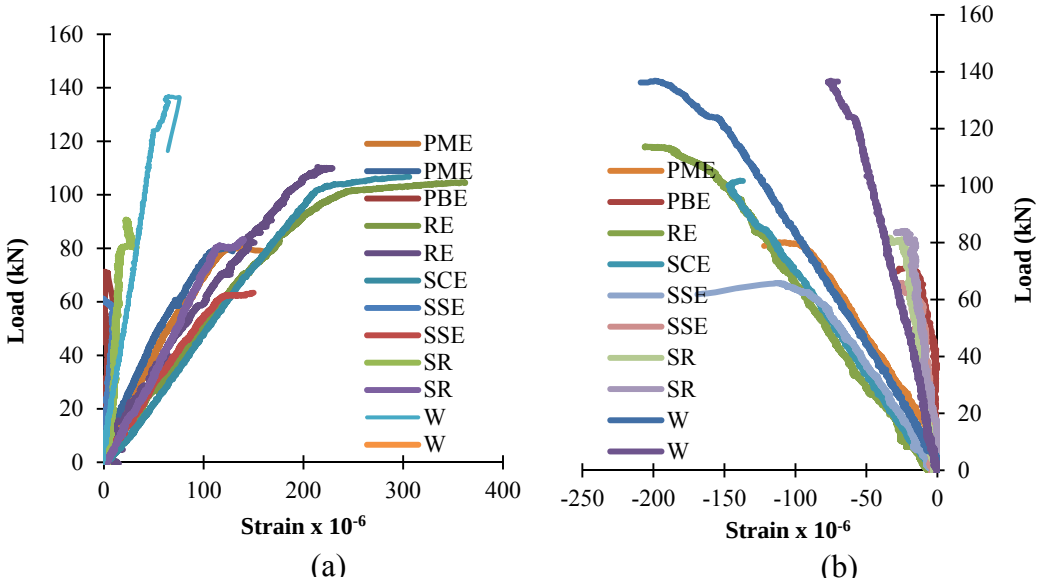

Figure 3-2. Measured load-strain curves for both lined and bare concrete pipes: (a) strain gauges at Locations 1 and 3 and (b) strain gages at Locations 2 and 4

As shown in Figure 3-2, some of the results do not have an acceptable trend which might be due to malfunction of the strain gauges. These results are eliminated in future analysis. Peak load for an unlined concrete pipe is 56 kN and the average peak load for lined concrete pipes with different linings is 88.4 kN, which represents an approximate 57% increase in the peak load.

3.2.2 Tensile Properties of Epoxy

ASTM-D638 (9) covers the methods to determine tensile properties of plastics in the form of standard dumbbell-shaped test specimens. A testing machine of the constant rate of cross head movement with one fixed member carrying the grip and a moveable member carrying the second grip is required. The machine used in this research is a Shimadzu AG-X plus universal tester, located in the Advanced Material and Structures Lab (AMSL) at the University of Texas at Arlington, Department of Mechanical

Engineering. Measurement of specimen elongation is performed by a Model 3542 axial extensometer from Epsilon Technology Corp, installed within the gauge length of the specimen.

A total of nine standard samples provided by Raven lining systems with a thickness of 2.8 mm were tested and a sample test result is presented in Figure 3-3.

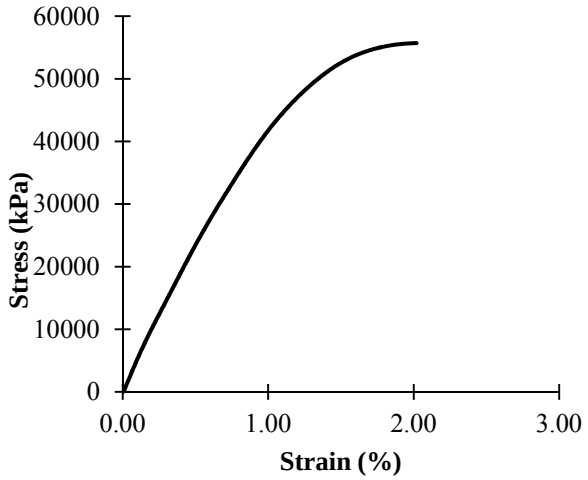

Figure 3-3. Stress-strain curve for Raven epoxy lining

The results obtained from the tests indicate an elasto-plastic behavior for the epoxy with a modulus of elasticity equal to 4,960 MPa. The results were used for lining simulation of coated concrete beams and lined concrete pipes.

3.2.3 Flexural Strength of Concrete

Flexural strength of concrete is determined by the use of a simple beam with third-point loading per ASTM-C78(10). According to the standard, two load applying blocks, each located at one third of the span length, must be in contact with the surface of the beam on top. The beam is centered on two support blocks. In this research a total of eight concrete beams, four of which were coated with Raven epoxy lining, are tested. Concrete beams are 56 cm x 15.2 cm x 15.2 cm, and for the case of coated concrete

beams, the thickness of the coating is 3 mm. The samples are coated by a certified specialist to the standards of the Raven lining systems at their own plant. Coating is sprayed on tensile side of the concrete beam after surface preparation.

Figure 3-4. shows prepared surface of the beams and coated concrete beams.

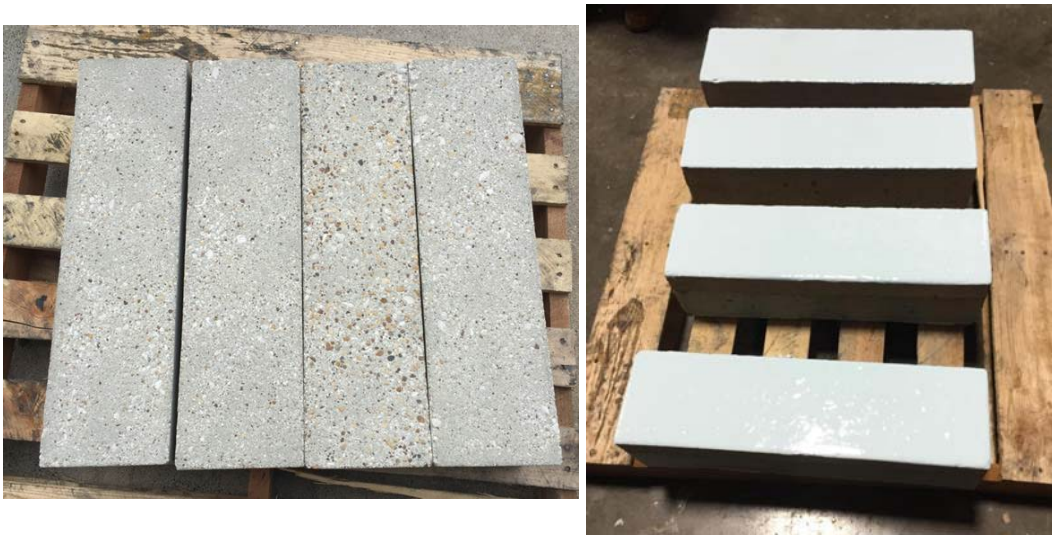

(a) (b)

Figure 3-4. (a) prepared surface for applying epoxy lining and (b) coated concrete samples (Photo by Elmira Riahi)

As shown in Figure 3-5 (a), samples are mounted on test set up with a span width of 45.7 cm, and two LVDTs are located on two sides of the beam at mid-span, to measure displacement of top of the sample due to the applied load. LVDTs and the loading frame are connected to data acquisition system and all measurements are transferred to an Excel worksheet. In order to capture the peak load and failure of the beam, a displacement control test with a rate of 0.1 mm/min is performed. The loading

frame is a 50 kips MTS machine. Displacement is applied until the sample is broken. Figure 3-5 (b) shows a broken concrete beam without coating.

(a) (b)

Figure 3-5. Flexural strength test on concrete beam: (a) test set up and (b) broken specimen (photo by Elmira Riahi)

Results obtained from the tests are shown in Figure 3-6. Comparison of the results for coated and uncoated concrete beams, indicate that an approximately 19% increase in the peak load is observed by applying a 3 mm epoxy to the concrete beam. The average maximum peak load from uncoated concrete beams is 40.1 kN, and the average maximum peak load for coated concrete beam is 47.6 kN.

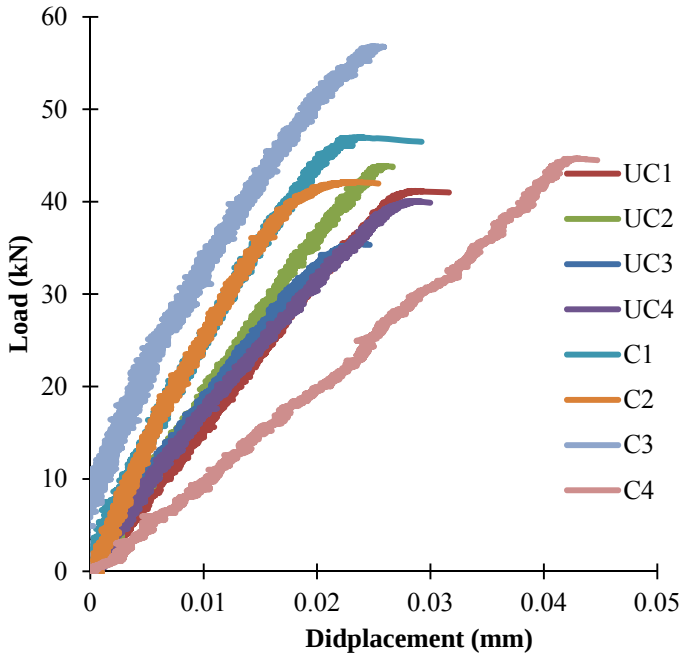

Figure 3-6. Comparison of the results from flexural strength test of coated and uncoated concrete beams

3.3 Finite Element Modeling

The multipurpose finite element software suit, ABAQUS was selected to simulate lined and unlined concrete pipes under D-load test. A three-edge bearing test was simulated in ABAQUS and the results obtained from the simulation were verified by test results. In order to create an accurate material behavior for concrete, test results from flexural strength tests were used to back calculate tension softening curves, which were then used in a concrete damaged plasticity model for concrete simulation in ABAQUS.

3.3.1 Material Model

For concrete simulation, the concrete damage plasticity (CDP) model available in ABAQUS material library was used. The model is a continuum, plasticity-based damage model for concrete. Since the two main concrete failure mechanisms are cracking under

tension and crushing under compression, evolution of the surface failure in the CDP model is controlled by plastic strains in tension and compression. According to the ABAQUS version 6.12 manual (11), this constitutive model aims to simulate post-peak behavior of concrete and other quasi-brittle materials under fairly low confining pressures. The plastic-damage model in ABAQUS is based on models proposed by Lubliner et al. (1989) (12) and by Lee and Fenves (1998) (13). Table 3-1. Concrete Material Properties presents the material properties of concrete used for the CDP model. Values presented in the table were obtained from test results or default values from the ABAQUS manual were used.

Table 3-1. Concrete Material Properties

Modulus of Elasticity (GPa)		30
Poisson Ratio		0.2
Density (kg/m^3)		2400
Plasticity	Dilation Angle (°)	38
	Eccentricity	0.1
	f_{b0}/f_{c0}	1.16
	K	0.667
	Viscosity Parameter (s)	10^{-7}

In Table 3-1, f_{b0}/f_{c0} is the ratio of initial equibiaxial compressive yield stress to initial uniaxial compressive yield stress (the default value is 1.16); K is the ratio of the second stress invariant on the tensile meridian to that on the compressive meridian at initial yield for any given value of the pressure invariant p such that the maximum principal stress is negative (11).

As mentioned in the test program, to define the material properties of the linings, test of tensile properties of plastics per ASTM D638 (9), was performed on samples

which were provided by one of the epoxy manufacturers participating in this research program (Raven Lining Systems, Tulsa, OK). After getting the test results, elasto-plastic material was selected for the lining. Available material properties of epoxy lining used for simulation are presented in Table 3-2.

Table 3-2. Material Properties of Epoxy Lining

	Elastic		**Plastic**	
	Modulus of Elasticity(MPa)	Poisson's Ratio	Yield Stress(kPa)	Yield Strain
Raven	4960	0.45	55	0.015
Warren	3450	0.45	48	0.048
Permaform	760	0.45	54	-

3.3.2 Tension Stiffening Curve

As part of the concrete damage plasticity model, post-peak behavior of the material must be provided in material definition. This behavior, which defines crack propagation in concrete, is modeled by using a tension stiffening curve (TSC), which allows simulation of strain-softening behavior of cracked concrete. Under uniaxial tension before reaching the failure stress, σ_t, the stress-strain response follows a linear elastic relationship. The failure stress is the beginning of micro-cracking in concrete material. After reaching the failure stress, formation of micro-cracks is represented macroscopically with a softening stress-strain response, which induces strain localization in the concrete structure. This behavior also allows the effects of the reinforcement interaction with concrete to be simulated in a simple manner. ABAQUS allows defining tension stiffening by means of a stress and cracking strain relationship or by applying a fracture energy cracking criterion (11). By using the results from flexural strength tests

on coated and uncoated concrete beams, tension-stiffening curves are established for both beams through optimization as shown in Figure 3-7 (a).

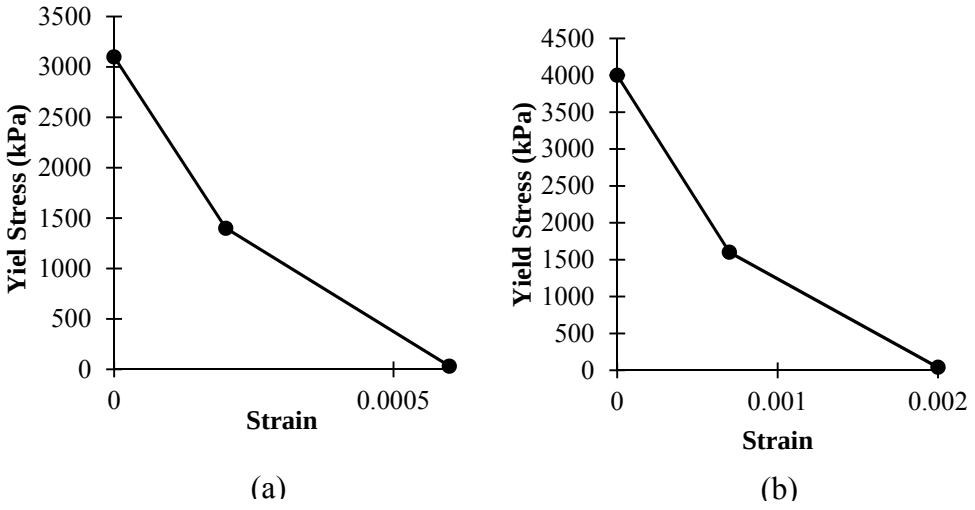

Figure 3-7. Tension stiffening curve for (a) concrete beam and (b) reinforced concrete pipe

Since the precast concrete pipes are reinforced, the tension stiffening curve used for their simulation is different from the tension stiffening curve obtained for unreinforced concrete beams. Figure 3-7 (b) shows the tension stiffening curve obtained for concrete pipes by using test results. The maximum strain for reinforced concrete is set to 0.002 which is the maximum strain for reinforcement. The maximum yield stress is also increased by 30% in order to consider reinforced concrete strength.

3.3.3 Interaction

Regarding the data provided by manufacturers, linings are perfectly attached to the concrete and in all of the pull-off tests conducted per ASTM D4541 (14) for epoxy lining, the failure mode was 100% concrete. As a result, for ABAQUS simulation, epoxy lining is attached to the concrete by using tie constraint. A surface-based tie constraint ties two surfaces together for the duration of a simulation. It constrains each of the nodes

on the slave surface to have the same motion as the closest point on the master surface (11). In this simulation, concrete is defined as the master surface and lining is set as the slave surface.

3.3.4 Flexural Strength Test on Concrete Beam

A simulation of flexural strength test of coated and uncoated concrete beams was performed in ABAQUS. The model is a three-dimensional concrete beam with 56 cm length and 15.2 cm x 15.2 cm cross section and an 8-node linear brick element type. To apply the boundary conditions, two rigid strips were located within 5 cm from the edges at the bottom of the beam, representing the supports, and two rigid strips are located on top of the beam, each at one third of the span length, representing loading noses. Rigid plates are used to avoid stress concentration in the beam. Rigid strips are tied to samples. A schematic illustration of the model is shown in

Figure 3-8.

Bottom supports are restricted from moving in y direction and top strips are constrained in x and z directions. After generating the model, a downward displacement of 0.1 mm is applied to the top strips. For the case of coated concrete beams, a layer of 3 mm epoxy lining is tied to the bottom of the beam. Results obtained from these simulations are verified by comparing the simulation results with the test results.

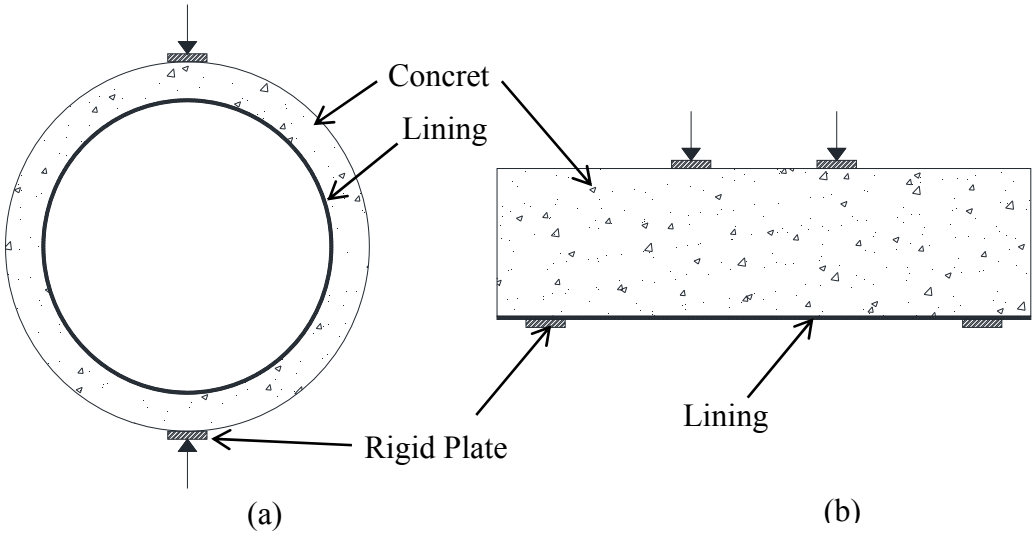

Figure 3-8. Schematic models generated in ABAQUS: (a) three-edge bearing test on concrete pipe and (b) flexural strength test of concrete beam

3.3.5. Three-Edge bearing Test on Concrete Pipes

A two-dimensional model of a pipe with 61 cm inside diameter and 7.6 cm thickness was generated in ABAQUS. Four-node bilinear plane stress quadrilateral elements (CPS4R) were used for pipe simulation. In order to avoid stress concentration at boundaries, two rigid plates were tied on the top and bottom of the pipe as shown in

Figure 3-8. The bottom plate was restricted from moving in x and y directions. The top plate was constrained in x direction and a downward displacement of 2.5 mm was applied on top of the pipe in y direction. For lined concrete pipe, the lining was tied inside of the pipe.

3.4 Results and Model Validation

Comparison of the results obtained from experiments and finite element simulation are presented to validate finite element model for further parametric studies of coated concrete members.

3.4.1 Beam Simulation

Results of four-point bending tests on uncoated concrete beams were close to each other, and one of the test results was selected and compared to the finite element simulation as shown in Figure 3-9. The peak load and crack formation in the simulation mirrored the results of the test observation.

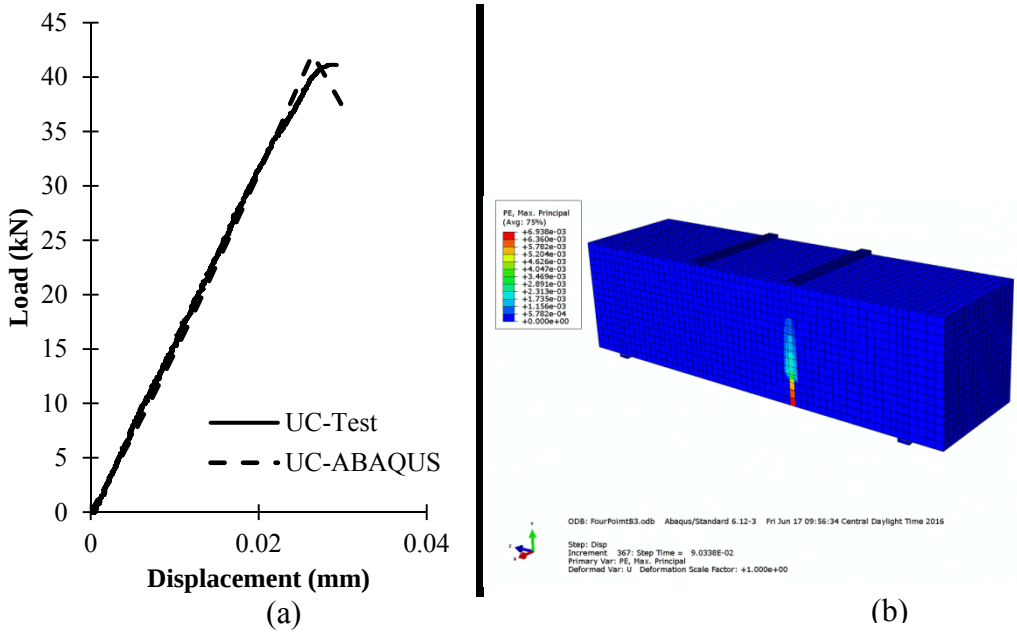

Figure 3-9. Uncoated concrete beam simulation shows (a) comparison to test results and (b) crack propagation

Test results from coated concrete beams vary in peak load and behavior. The simulation was performed to obtain the best results which as presented in Figure 3-10 (a). The peak load obtained from FEM simulation is close to the results obtained from

the test, while the test results have stiffer behavior compared to the finite element model. This difference may be caused by boundary conditions or mesh size. Crack propagation in the coated concrete beam is shown in Figure 3-10 (b) which is the same as that observed in the test results.

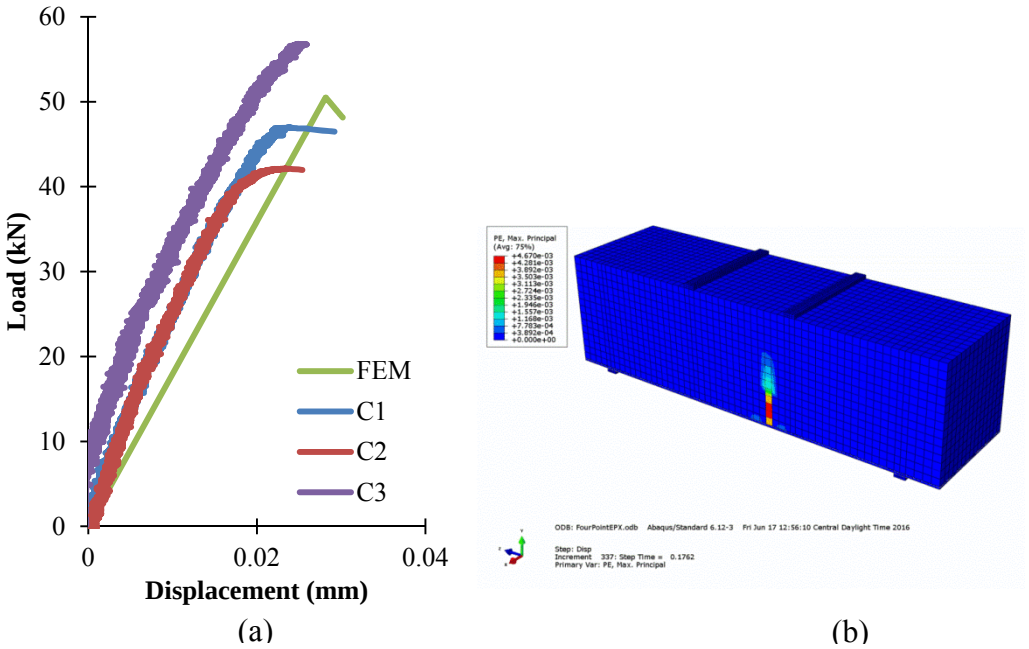

Figure 3-10. Coated concrete beam simulation: (a) comparison to test results and (b) crack propagation

3.4.2 Concrete Pipe Simulation

As shown previously, the experimental results from lined and unlined concrete pipe cover a wide range of variations in peak loads for different types or thicknesses of lining materials. Since the database of the experiments is not completely available, only selected data is shared here for model validation.

Crack formation in the unlined concrete pipe in finite element simulation is shown in Figure 3-11. The order of crack propagation in the finite element model is the same as

crack propagation in the experiment; hence, the cracks on top and bottom of the inner face of the pipe are formed first and the cracks on the sides are formed later.

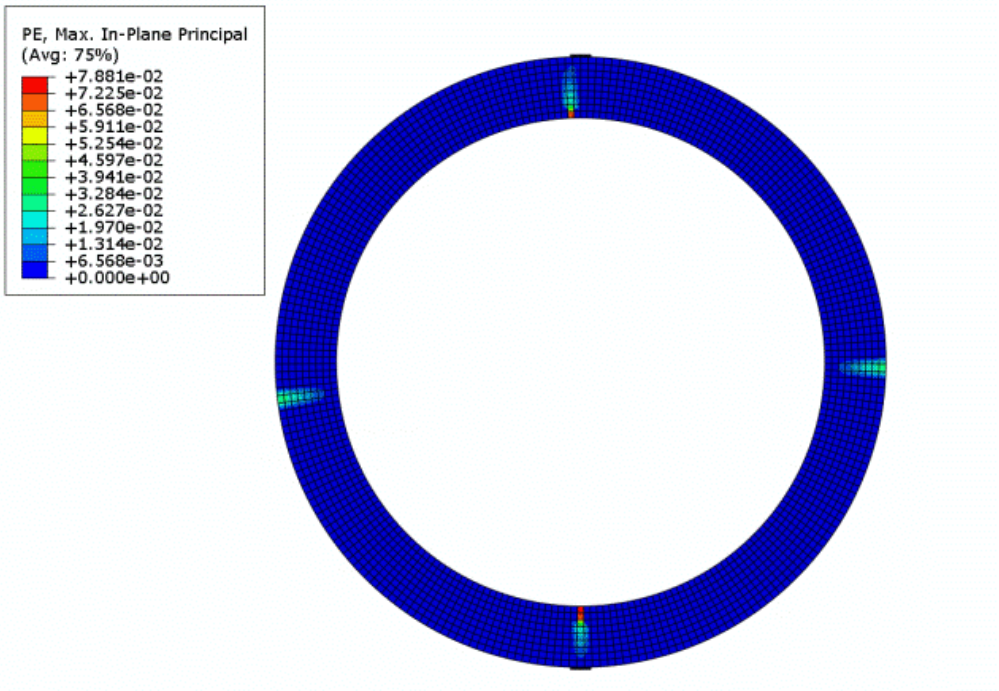

Figure 3-11 Crack formation in unlined concrete pipe

Comparison of the test results with the simulation for load-strain curves are presented in Figure 3-12. As shown, the finite element model has closely predicted the behavior of the unlined concrete pipe. As mentioned previously locations 1 to 4 refers the location of the strain gauges installed inside of the pipe. Strain gauges 1 and 3 are located at top and bottom of the pipe and strain gauges 2 and 4 are located at two sides of the pipe.

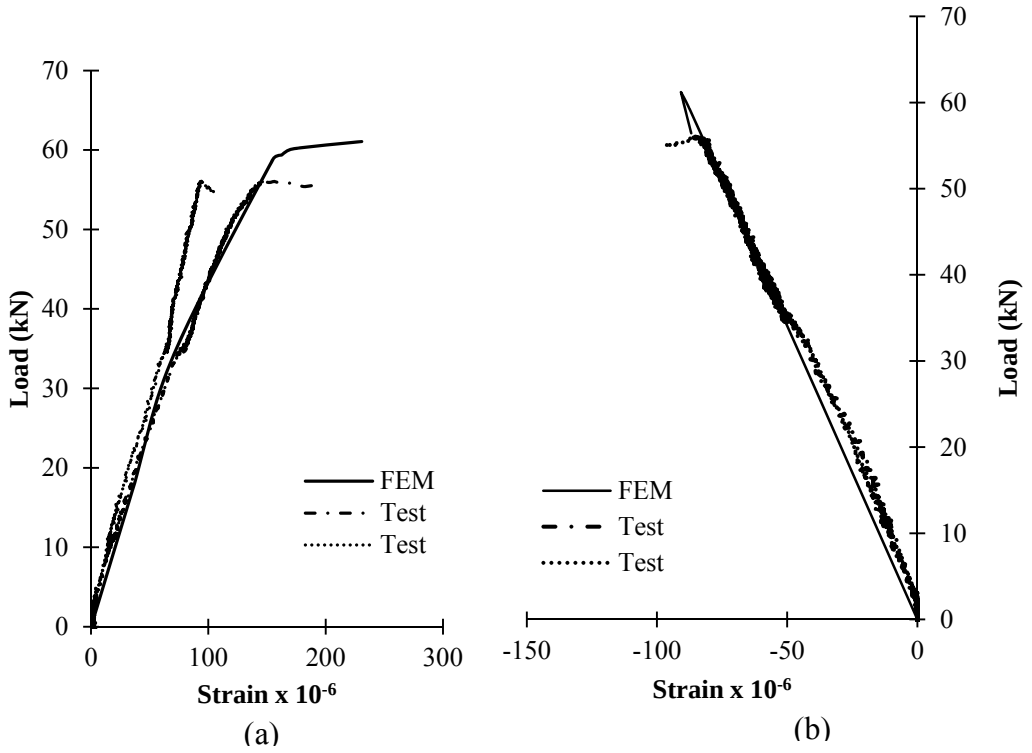

Figure 3-12 Comparison of measured and simulated load-strain curves for unlined concrete pipes: (a) strain gauges at Locations 1 and 3 and (b) strain gages at Locations 2 and 4

Figure 3-13 compares the results from selected lined concrete pipe with finite element simulation. As shown for the selected cases, finite element simulation results are in good agreement with the results obtained from the experiment. The peak loads are almost the same while slightly larger strain is observed in the simulation.

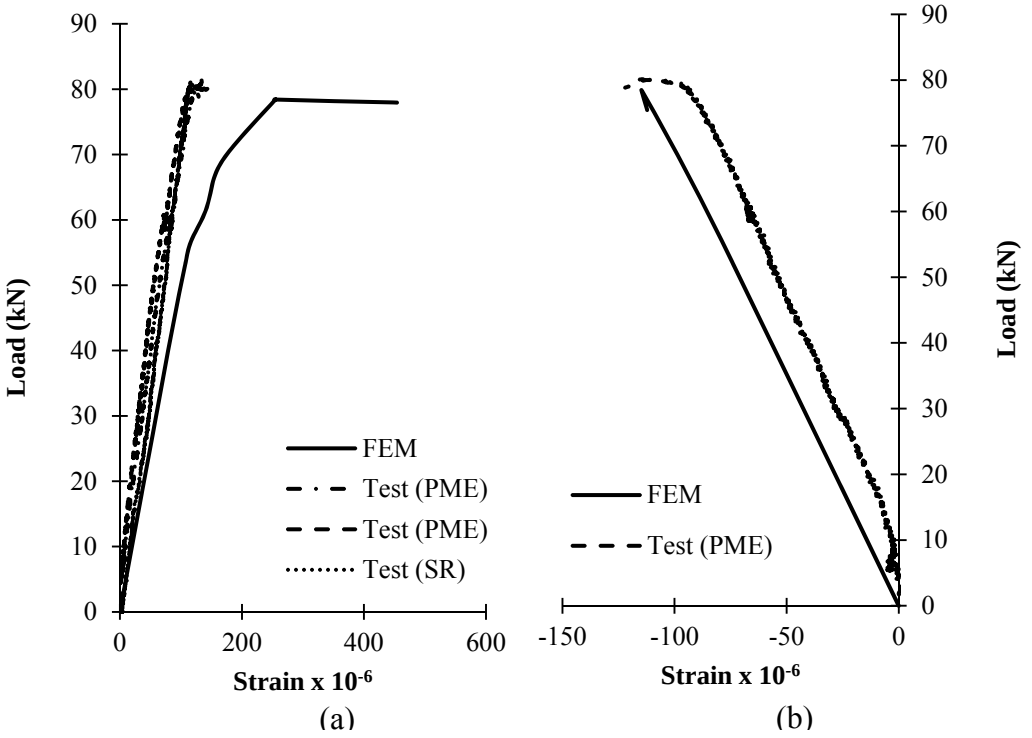

Figure 3-13 Comparison of measured and simulated load-strain curves for selected lined concrete pipes: (a) strain gauges at Locations 1 and 3 and (b) strain gages at Locations 2 and 4

3.5 Parametric Study

After validation of the model, it can be used for parametric study on behavior of the lined concrete pipe under D-load configuration. Stiffness of concrete and the lining, which are controlled by changing their Young's modulus, and thickness of the lining are the parameters set apart for specialized study in this research. For each parameter the peak load and radial deformation at peak load were compared.

Figure 3-14 presents variation of the peak load with thickness of the lining for different Young's modulus values in concrete. Different values of Young's modulus can be representative of different degrees of degradation of concrete pipe. Figure 3-14 shows three different percentages of Young's modulus, 100% E, 50% E and 30% E in which E is the original Young's modulus of the concrete. The simulation for different Young's

modulus was performed for three different linings, each with a different thickness, that is, 3 mm, 6 mm and 12 mm. One case without lining was also considered as a base point for comparison. For all cases by increasing the thickness of the lining the peak load increases. Degradation of the concrete pipe slightly changes the peak load for each case. For the case of 30%E, variation of the peak load with thickness of the lining is different from the other two cases. In this case adding a layer of 3mm of lining does not increase the peak load compared to the case without any linings, while a sudden increase of about 40% is observed after increasing the lining thickness to 6mm.

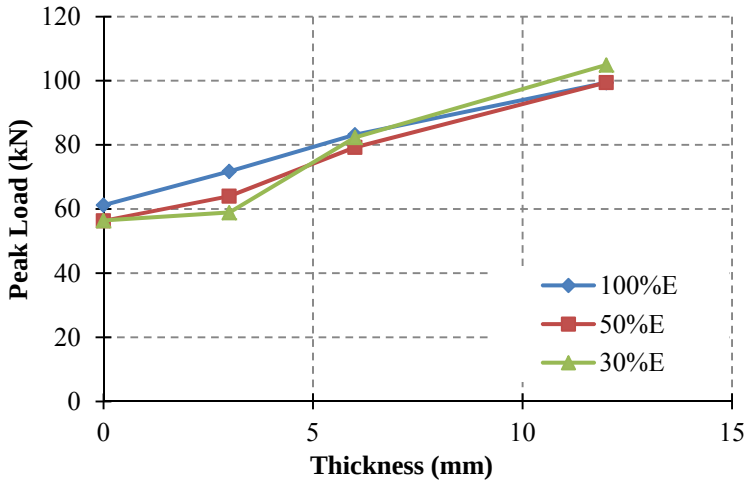

Figure 3-14. Variation of the peak load with thickness of the lining for different Young's modulus of concrete

Comparison of radial deformation at peak load for different thicknesses of the lining and Young's modulus of the concrete pipe is shown in Figure 3-15. By decreasing Young's modulus, stiffness of the concrete decreased and larger deformations were observed in the pipe. Since the peak load is increasing by increasing the lining thickness, for thicker linings larger deformations are recorded.

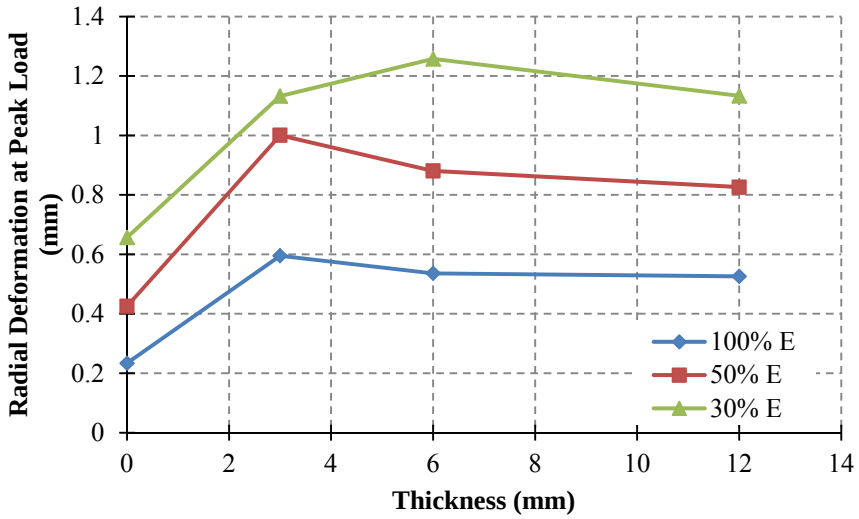

Figure 3-15. Variation of radial deformation with thickness of the lining for different Young's moduli of concrete

To study the effect of material properties of the lining, one additional case with a lining that has half of the Young's modulus of the original lining is simulated. Comparison of the results for different combinations of concrete and lining stiffness values are shown in Figure 3-16. In the legend E_l and E_c represent Young's modulus of lining and concrete, respectively. Reducing the stiffness of the lining decreases the peak load obtained from three-edge bearing test simulation.

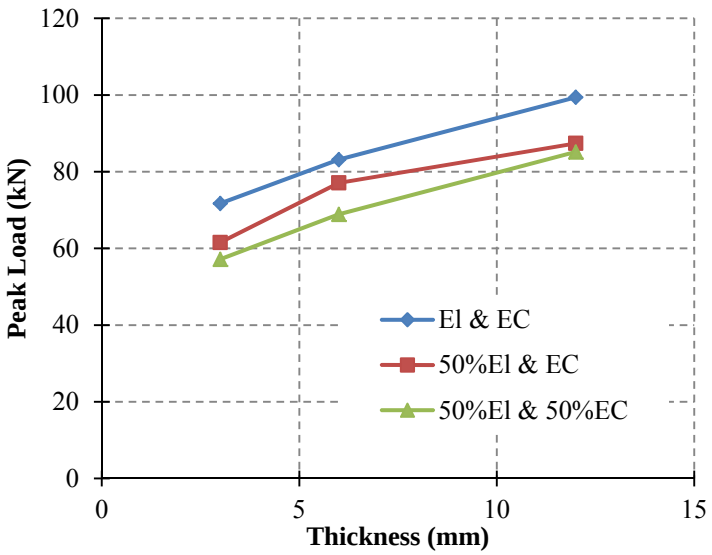

Figure 3-16 Variation of the peak load with thickness of the lining for different Young's modulus of concrete and lining

For the case described above, variation of radial deformation at peak load is shown in Figure 3-17. By increasing the thickness of the lining, radial deformation decreases. For the case of 50% E_l and 100% E_c, radial deformation at peak is almost constant for lining thickness of 3 mm and 6 mm, while using a lining with thickness of 12 mm reduces deformation by 14%. A large increase of deformation is also observed for the case of using 50% Young's modulus for both concrete and lining.

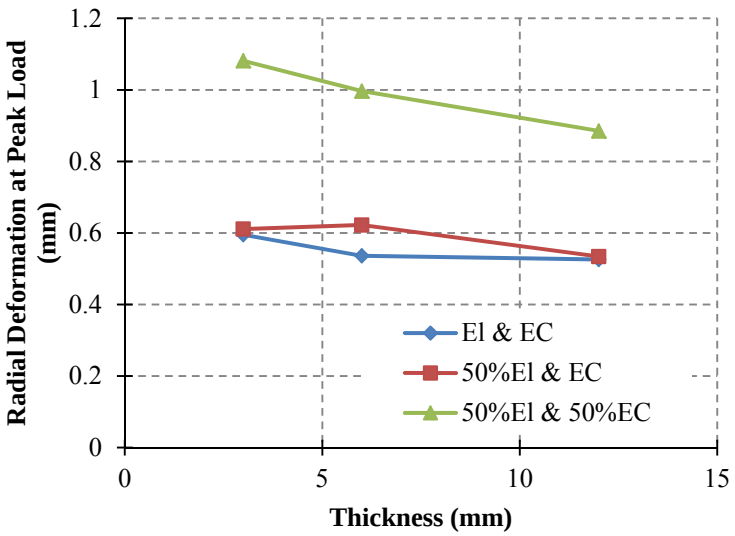

Figure 3-17 Variation of radial deformation with thickness of the lining for different Young's modulus of concrete

For the case of original Young's modulus of the concrete and reduced Young's modulus of lining material, radial deformation at peak remains the same as the case with original modulus for both lining and concrete lining with thickness values of 3 mm and 1 2 mm, but the radial deformation peak slightly increases for 6 mm thick lining.

3.6 Conclusion

Two different sets of tests on concrete with and without lining are used to study behavior of composite concrete members. The results from flexural strength test on concrete beams and three-edge bearing tests on concrete pipes are used to generate a finite element model of three-edge bearing tests on unlined and lined concrete pipes. The calibrated model is used to perform a parametric study on composite concrete pipes under D-load configuration. Effect of variation of several parameters on peak load and radial deformation of the pipe at peak load is considered in this study. Different Young's

modulus values of the concrete as a representative of degree of degradation of concrete pipe as well as different Young's modulus values and thickness of lining material are parameters used for parameter study of the composite pipe.

The results obtained from the simulation indicate that, increasing the thickness of the lining increases the peak load and by reducing the Young's modulus of the concrete to 30% of the original Young's modulus, the effect of lining thickness on peak load and radial deformation of the pipe increases. Reduction in Young's modulus of the lining material decreases the peak load, and with reduced modulus of concrete, large deformations are observed for different lining thicknesses.

References

1. Sanchez-Silva M, Rosowsky DV. Biodeterioration of Construction Materials: State of the Art and Future Challenges. Journal of Materials in Civil Engineering. 2008;20(5):352-65.

2. Mahmoodian M, Alani A. Modeling Deterioration in Concrete Pipes as a Stochastic Gamma Process for Time-Dependent Reliability Analysis. Journal of Pipeline Systems Engineering and Practice. 2014;5(1):04013008.

3. Water Research Foundation, prepared by Davies JP, Clarke BA, Whiter JT, Cunningham RJ. Factors influencing the structural deterioration and collapse of rigid sewer pipes. Urban Water. 2001;3(1–2):73-89.

4. Abraham DM, Ali Gillani S. Innovations in materials for sewer system rehabilitation. Tunnelling and Underground Space Technology. 1999;14, Supplement 1:43-56.

5. Dan Ellison FS, Peter Oram, Will Lovins, and Andrew Romer,Steven J. Duranceau,Graham Bell. Global Review of Spray-On Structural Lining Technologies. 2010.

6. Mohammad Najafi VFS. STRUCTURAL CAPABILITIES OF NO-DIG MANHOLE REHABILITATION. 2015.

7. Standard Test Methods for Concrete Pipe, Manhole Sections, or Tile (Metric). ASTM International; 2015.

8. Standard Specification for Reinforced Concrete Culvert, Storm Drain, and Sewer Pipe. ASTM International; 2015.

9. Standard Test Method for Tensile Properties of Plastics. ASTM International; 2014.

10. Standard Test Method for Flexural Strength of Concrete (Using Simple Beam with Third-Point Loading). ASTM International; 2016.

11. Hibbit, Karlsson, Sorensen. ABAQUS/Standard Analysis User's Manual: Hibbit, Karlsson, Sorensen Inc.; 2007.

12. Lubliner J, Oliver J, Oller S, Oñate E. A plastic-damage model for concrete. International Journal of Solids and Structures. 1989;25(3):299-326.

13. Lee J, Fenves G. Plastic-Damage Model for Cyclic Loading of Concrete Structures. Journal of Engineering Mechanics. 1998;124(8):892-900.

14. Standard Test Method for Pull-Off Strength of Coatings Using Portable Adhesion Testers. ASTM International; 2009.

Chapter 4

Structural Behavior of Epoxy-Coated Rehabilitated Concrete Manhole Structure

4.1 Introduction

Manholes are access points to infrastructures such as sewer and drain systems and they play an important role in inspection and maintenance of underground structures. Manholes may experience structural decay during their service life which must be addressed in an efficient way to avoid failure and catastrophic consequences such as sinkholes. Trenchless technology, also referred to as the “No-dig” manhole rehabilitation method, is one of the various existing methods to rehabilitate deteriorated manhole structures. In this method a layer of lining is applied inside of the manhole structure to fill in the cracks and restore the structure’s integrity. Ever since this method was first used, structural capacity of the lining has been ignored. This research studies structural behavior of epoxy-coated manhole structures by creating a finite element model which is validated by the results from an existing full-scale manhole experiment. A calibrated model was used to do parameter study on effect of epoxy lining on deteriorated concrete manhole structure under soil, water and traffic loads. In addition to the existing Mohr-Coulomb material behavior model, the Duncan-Chang constitutive model, was implemented in ABAQUS finite element software as a subroutine for soil simulation. The results from this study show that for the chosen manhole height with the applied loads and considered degrees of concrete deterioration, epoxy lining does not have a significant effect on structural capacity of the manhole structure.

Maintenance and inspection of underground structures is performed through manholes which are access points to infrastructures. Manholes are usually circular pipes in various sizes which are placed in the soil vertically. These structures are usually made

of bricks or concrete. Since these structures are the main entrance to underground structures, it is vital to keep them sound and trustworthy during their service life. However, regarding their surrounding environment manhole structures can be easily in the risk of deterioration. The main reasons for manhole deterioration can be inflow of water during rain, infiltration of groundwater through cracks, fractures and loose joints, corrosion due to exposure to aggressive environment such as sulfate attack and chloride ion penetration, formation of cracks or fractures as a result of poor construction, inferior materials and external loads (1).

According to the United States Environmental Protection Agency (USEPA), there are 20 million manholes in the United States and 3.5 million of them are suffering from serious structural decay. There are several different ways to address manhole deterioration such as casting new permanent or removable internal lining, sprayed cast concrete or polymer lining, cured-in-place linings, grouting and sealing approaches (2). According to type and degree of structure deterioration, an appropriate method must be chosen for rehabilitation. Different parameters dictate the type of rehabilitation method. Cost, feasibility, existing loads, surrounding environment, expected service life and residual strength of the deteriorated manhole are some of these parameters. Sprayed cast polymer linings are widely used for manhole rehabilitation due to their ability to achieve one-day return to service, minimal community impacts, and low installation costs. In this method a layer of polymer lining such as epoxy or polyurethane is spayed inside the manhole structure. Despite its popularity, the spray-on polymer lining as a means of rehabilitation has not had its structural benefits analyzed from the aspect of structural strength and integrity. These linings have always been categorized as a “non-structural” rehabilitation method (3).

In order to study the structural capacity of a sprayed-on polymer lining rehabilitated manhole structure, full-scale manhole experiments and numerical modeling is required. Several experimental studies have been conducted to evaluate different properties of manhole rehabilitation materials (4)–(5). However, to the best of this author's knowledge, an in-depth research project on numerical modeling of manhole structures is limited. A doctoral research by Sabouni (2008) studied loading/deformation conditions on precast concrete manholes. Laboratory tests on three full-scale precast concrete manholes and finite element simulation, using PLAXIS software were performed in this research. Results from Sabouni et al. experiments can be used as a reference on the state of strains in the manhole and stresses in the surrounding soil (6). A comprehensive parametric study on behavior of the circular precast concrete manhole structure in different conditions was performed by the means of finite element simulation (7). Performance of cured-in-place pipe lining rehabilitation method was evaluated by J. Matthews et al. by performing a comprehensive field and laboratory tests, which is presented in a report published by USEPA in 2012 (8). According to the report, the project was a successful demonstration of an innovative Class IV (fully structural) water main rehabilitation technology.

In order to study the structural capability of No-dig manhole rehabilitation method, Water Environment Research Foundation (WERF) in 2015, performed a comprehensive laboratory and finite element simulation on structural behavior concrete lined with different types of linings. The results of this project suggest that any type of manhole rehabilitation material can be applied as fully structural; nevertheless, it may be difficult to achieve the thickness required to qualify as fully structural for the spray-applied, cured-in-place type liners (9).

In this research a finite element model of a concrete manhole structure is generated in ABAQUS, multipurpose finite element software. The generated model is calibrated by using the results from a set of full-scale manhole experiments from Sabouni's doctoral research in 2008 (10). In the finite element model a layer of epoxy coating is applied inside of the manhole with different degrees of deterioration of concrete and structural behavior of the composite structure under soil, water and traffic load is studied. To study the effect of soil pressure on manhole structure two different soil constitutive models, Mohr-Coulomb and Duncan-Chang, are used for simulation and the results are compared.

4.2 Existing Full-Scale Manhole Experiment

In the full-scale manhole experiment, two manholes with reinforced concrete and inside diameter of 1.2 m and 1.5 m and one non-reinforced manhole with 1.2m are instrumented and tested under lateral soil pressure and different traffic load configurations in a large scale geotechnical testing facility (LSGTF) located in the structure laboratory of the University of Western Ontario (Western) (6). In current research only the unreinforced 1.2 m manhole is used for simulation and model verification.

As shown in Figure 4-1, the concrete manhole consists of one 1.2 m high monobase, four risers, and one tapered top. The monobase has a non-reinforced base with a thickness of 150mm and wall thickness of 139mm with a 1.219m inner diameter. The total height of the manhole is 5.89m and height of each manhole part is illustrated in Figure 4-1. The manhole was tested in a soil pit with rigid walls and floor. The soil test pit had a base of 4.5m by 4.5m and height of 7.26m. A layer of 0.65m sand was located at the bottom with a layer of 0.3m gravel on top of that. The manhole base was placed on the gravel layer and the manhole walls were surrounded by 5.33m concrete sand. The top layer was

0.53m thick gravel (6). The manhole was installed following the standard installation procedure specified by the Ontario provincial standard specification (11) (OPSS 402 former 516) (MTO and MEA 2005)

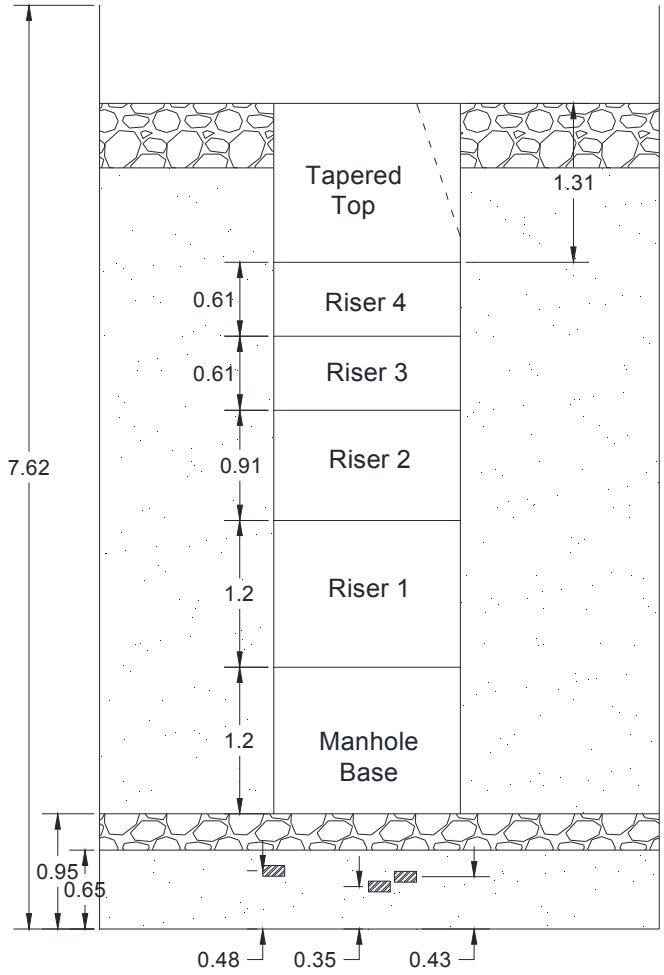

Figure 4-1: Physical full scale manhole laboratory test (units in m)

4.3 Finite element model

4.2.1 Manhole

Finite element simulation is performed using a multipurpose finite element software suite, ABAQUS. The simulation was performed by following all the procedures

in the experiment. A two-dimensional axisymmetric model is generated in ABAQUS. A 4-node bilinear axisymmetric quadrilateral, reduced integration, hourglass control (CAX4R) element was used to model both the concrete and the soil. In the initial step the layer of sand and gravel beneath the manhole are modeled and geostatic stress is obtained for those two layers. Stage construction is started by adding the monobase and sand layer with 1.21 m height. Each stage is defined in the model as one step in which the soil layer and the manhole riser is activated. The interaction between the soil and concrete is modeled using a frictional model with normal and tangential behavior. The friction formulation used for tangential behavior is “Penalty” with a friction coefficient of 0.8 for interaction between soil and manhole and 0.3 for interaction between soil and rigid wall. Due to lack of data on condition and roughness of the manhole and rigid wall, aforementioned values are obtained by performing several simulations with different combinations of the friction coefficients and comparison of the results with actual test conditions. The normal behavior is modeled with “Hard” contact pressure over closure approach, without allowing separation after contact. The tapered part of the manhole is ignored since it does not affect the results significantly (7). The geometry and mesh used for the model is shown in Figure 4-2.

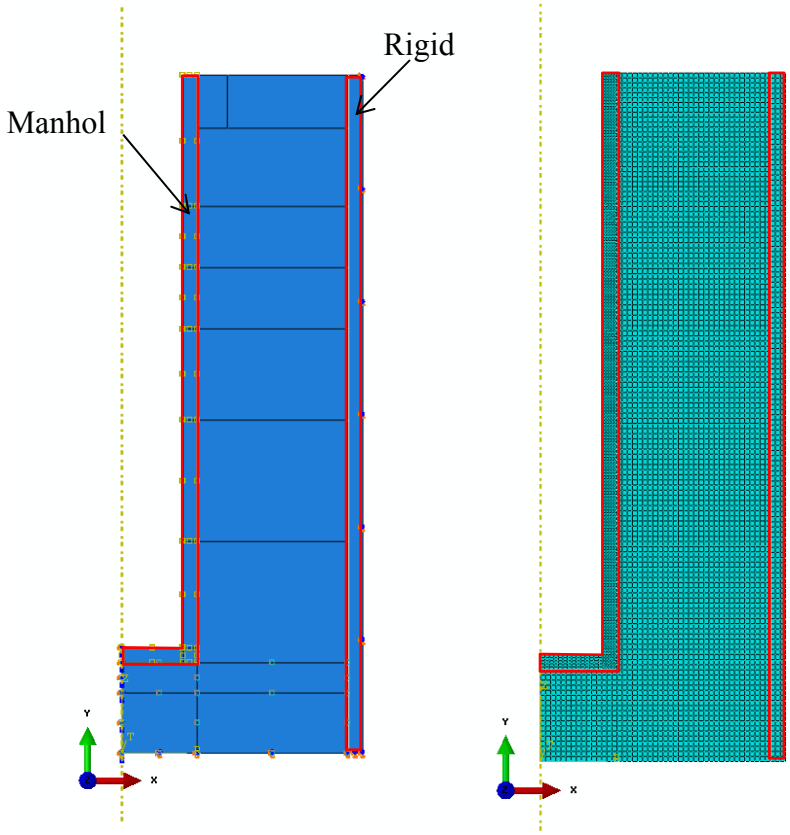

Figure 4-2. Geometry and mesh from ABAQUS simulation

The rigid wall of the test pit is simulated on the right side of the soil mass. The boundary condition used in the model restricts the rigid wall movement in vertical and horizontal directions on the right. At the bottom, the same as the rigid wall, the soil is restricted to move in all directions and on the left an axisymmetric boundary condition is applied.

The simulation is performed by considering two different types of soil behavior. Mohr-Coulomb model, which is an elastic perfectly plastic model, is used as an existing material model in ABAQUS. To improve the results Duncan-Chang model is also implemented as a subroutine in ABAQUS simulation. Duncan-Chang (hyperbolic) model

is a nonlinear model with a stress-dependent stiffness (12). Both of the simulations have the same geometry and the only difference is in the soil behavior applied in each case.

Material properties used for soil in each case are presented in Table 4-1. For the Mohr-Coulomb model, properties are obtained from test results presented in a full scale manhole experiment. For the Duncan-Chang model since there is no test data available; hence, the value of different parameters is obtained by creating a unit cube in ABAQUS and performing a true triaxial test using the available Mohr-Coulomb material properties and calibrating the results for Duncan-Chang material properties.

Table 4-1 Soil properties

Model	Soil Type	Unit Weight (kN/m^3)	Modulus of Elasticity (kPa)	Angle of internal Friction (°)	R_f	K	K_b	K_{ur}	n	m
Mohr-Coulomb	Sand	19	$5.2x10^5$	39	-	-	-	-	-	-
	Gravel	23	$6.8x10^5$	42	-	-	-	-	-	-
Duncan-Chang	Sand	19	-	39	0.9	3000	2400	3300	0.54	0.6
	Gravel	23	-	42	0.9	4200	4000	5000	0.54	0.6

- C is zero for all soil types

In the Duncan-Chang model a hyperbolic stress-strain function, based on Kondner's (13) idea, is used to describe the deviatoric stress-axial strain curve obtained from triaxial tests. This relationship is shown in Eq. (1).

$$\sigma_1 - \sigma_3 = \frac{\varepsilon}{a+b\varepsilon} \quad (1)$$

In which σ_1 and σ_3 are the major and minor principle stresses, ε is the axial strain and "a" and "b" are experimentally determined constants. As shown in Eq. (2), Failure ratio, R_f, relates the asymptotes in Figure 4-3 to compressive strength.

$$(\sigma_1 - \sigma_3)_f = R_f(\sigma_1 - \sigma_3)_{ult} \quad (2)$$

The value of R_f for different soils has been found to be between 0.75 and 1.00, and it is essentially independent of confining pressure.

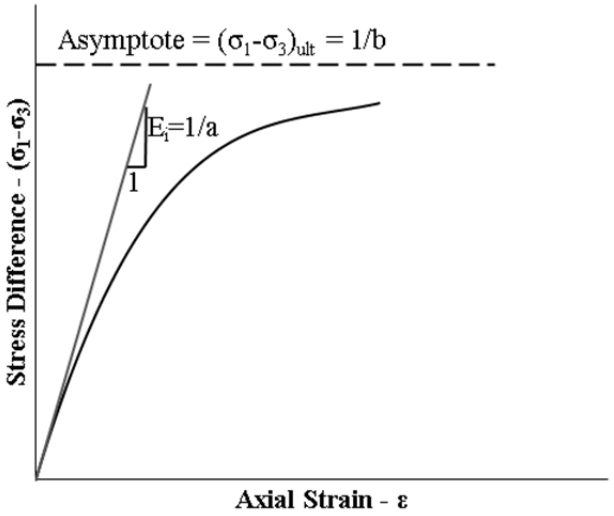

Figure 4-3: Hyperbolic stress-strain curve

As a matter of fact, this model has been found to be a convenient and useful means of representing the non-linearity of soil stress-strain behavior. Both the tangent modulus value and compressive strength of soils have been found to vary with the confining pressure employed in the tests, except in the case of unconsolidated-undrained tests on saturated soils. Janbu (14) has shown that the relationship between initial tangent modulus and confining pressure may be expressed as:

$$E_i = Kp_a(\frac{\sigma_3}{p_a})^n \quad (3)$$

where E_i is the initial tangent modulus, and p_a is the atmospheric pressure. K modulus number and n the exponent determine the rate of variation of E_i with σ_3, the minor principal stress. Both K and n are pure numbers and their values can be determined by plotting the values of E_i against σ_3, obtained from a series of tests, which are on log-log scales and fit a straight line to the data (12).

K_{ur}, K_b and m are other parameters defined in the FORTRAN subroutine used for a material model implemented in ABAQUS for soil. K_{ur} is the unloading-reloading moduli to calculate tangential Young's modulus in this stage. K_b and m are moduli and exponent, which determine the rate of variation of moduli with confining pressure, respectively, for calculating tangential bulk modulus(15).

Concrete simulation is performed by using the concrete damaged plasticity model (16) existing in the ABAQUS material library. Table 4-2 presents the parameters required to define the manhole structure material model. Values in Table 2 are obtained from laboratory tests on concrete samples or they are extracted from the literature.

Table 4-2 Concrete Material Property

Modulus of Elasticity (GPa)		36
Poisson Ratio		0.2
Density (kg/m^3)		2400
Plasticity	Dilation Angle (°)	38
	Eccentricity	0.1
	f_{b0}/f_{c0}	1.16
	K	0.667
	Viscosity Parameter (s)	10^{-7}

Note: fb0=fc0 = ratio of initial equibiaxial compressive yield stress to initial uniaxial compressive yield stress (the default value is 1.16); K = ratio of the second stress invariant on the tensile meridian, to that on the compressive meridian, at initial yield for any given value of the pressure invariant p such that the maximum principal stress is negative.

4.2.2 Pipe Under Uniform Peripheral Pressure

Regarding the nature of load acting on the manhole structure, which is a uniform circumferential compression load in most cases, a finite element simulation was performed on a 2D pipe in which a uniform peripheral compressive pressure was applied on the pipe. In ABAQUS the load was applied by assigning uniform radial displacement on the outer surface of the pipe. A two-dimensional pipe with an inner diameter of 61 cm

and thickness of 7.6 cm was created in ABAQUS. Behavior of lined concrete pipe under compressive load configuration is studied by adding a layer of 6 mm lining inside of the pipe. Schematic lined pipe under compression is shown in Figure 4-4. To verify the results from this simulation, elastic theory for pipe under peripheral pressure is used (17). Theory and the results are presented in model validation.

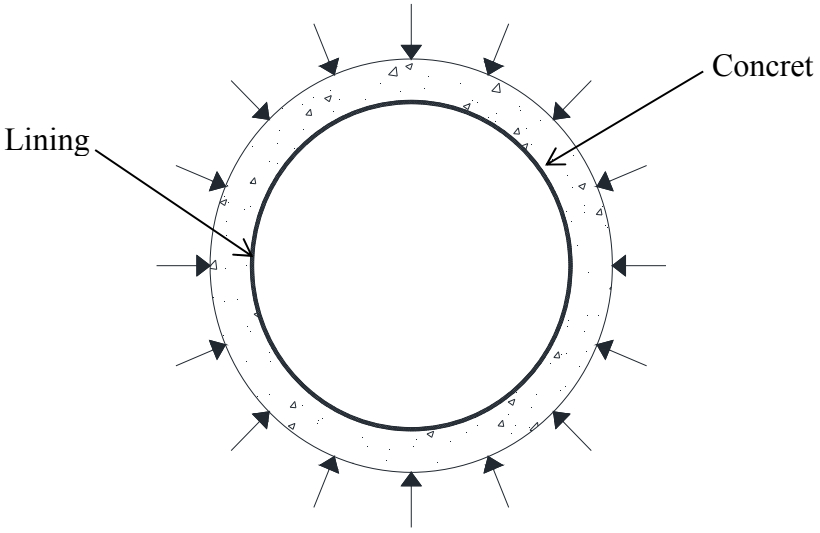

Figure 4-4: Schematic drawing of lined concrete pipe under compression

4.3 Model Verification

4.3.1 Soil Pressure Distribution Under Manhole Base

Pressure distribution contour under the manhole base (the red area in Figure 4-5) for Mohr-Coulomb and Duncan-Chang simulations are shown in Figure 4-5.

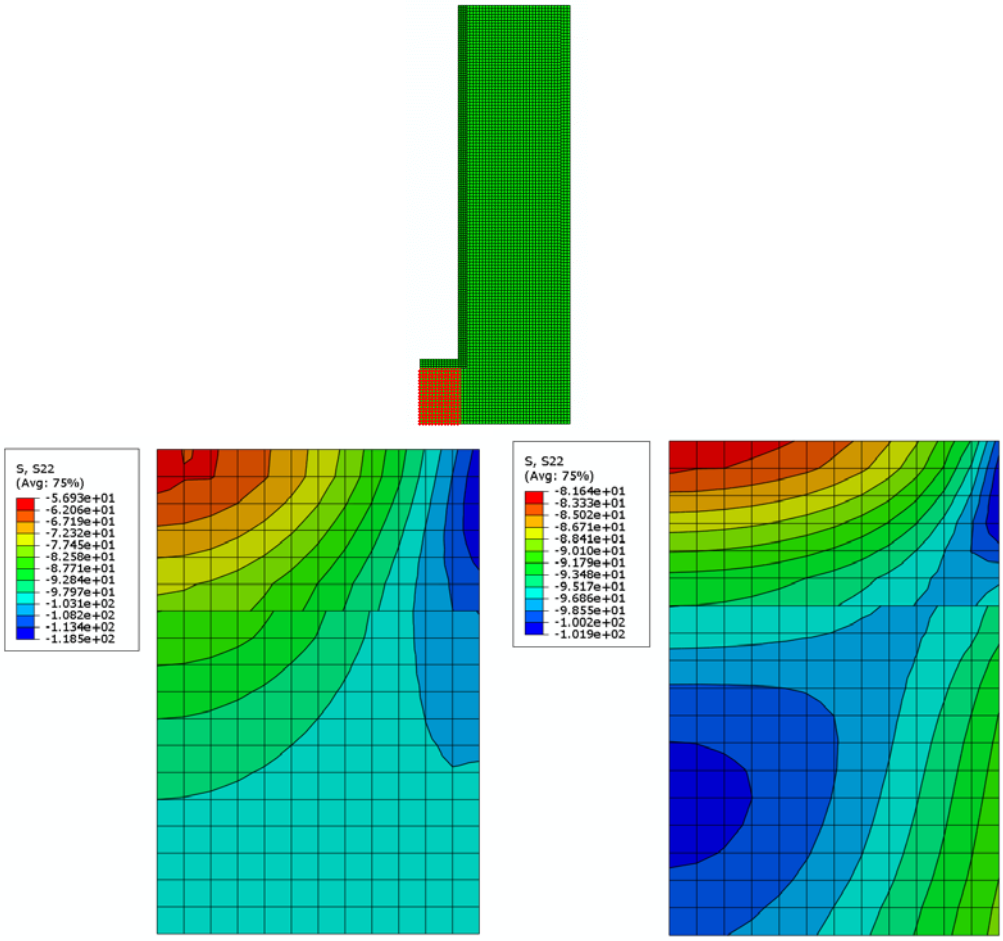

(a) (b)

Figure 4-5 Pressure distribution contour under manhole
(a) Mohr-Coulomb (b) Duncan-Chang
(b)

In the full-scale manhole experiment, as shown in Figure 4-1, no pressure cell located under the manhole base and the only available data for pressure distribution under the manhole is from a PLAXIS simulation performed by Sabouni et al.(7). As shown in Figure 4-6 and according to PLAXIS, simulation pressure at the center of the manhole base is smaller than the pressure under manhole walls. The same pattern is obtained from ABAQUS manhole simulation. In ABAQUS simulation for Duncan-Chang (DC) material model of soil, the minimum pressure under the manhole is about 80 kPa, and for Mohr-Coulomb (MC) material model this value is around 50 kPa which is close to

the results obtained from PLAXIS model. As shown in Figure 4-6, variation of pressure under the manhole base in the case of DC model is smaller than the other two cases.

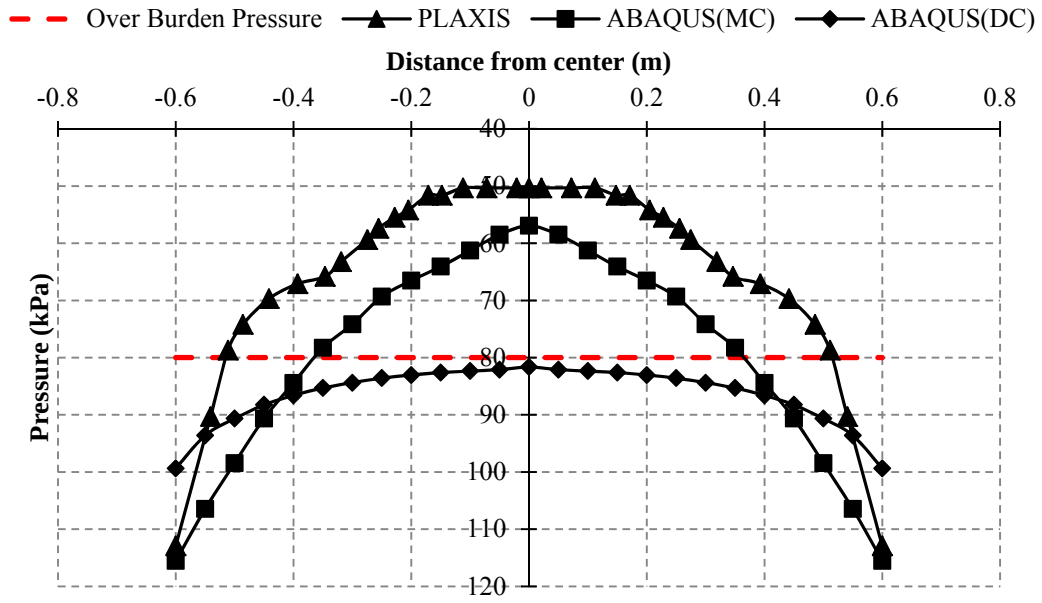

Figure 4-6: Pressure distribution under the manhole base

4.3.2 Pressure Distribution at 0.6 m Under Manhole Base

Three pressure cells are located at the center and under the wall of a manhole at a depth of 0.6 m. Pressures recorded by these cells are shown as red dots in Figure 4-7. It is observed that at this depth, pressure is smaller at the center and increases by moving toward the walls. For PLAXIS simulation at this depth only the pressure at the center and under the walls are reported (7). In ABAQUS simulation, for the DC material model, the pressure distribution pattern is the same as the experiment results with around 13% difference in magnitude at the center and less than 1% difference under the walls. On the other hand, using the MC material model for soil, results in a pressure pattern different from the experiment.

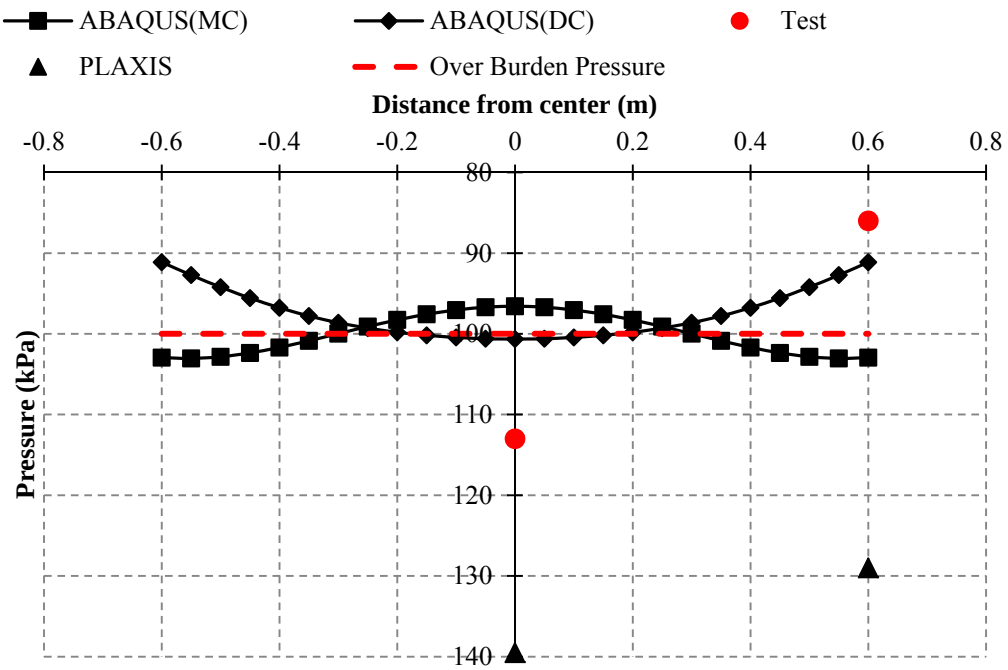

Figure 4-7: Pressure distribution at a depth of 0.6m under the manhole base

4.3.3 Lateral Soil Pressure

Figure 4-8 compares lateral soil pressure acting on the manhole structure. A pressure cell located at a depth of 1.44 m has recorded a pressure of 10.2 kPa, which is shown as a red dot in Figure 4-8. Lateral soil pressure is also calculated using at rest earth pressure theory. As shown in Figure 4-8 the results obtained from MC material model are close to the result obtained from pressure cell and the results obtained from at rest earth pressure theory are close to the DC material model simulation. Comparison of all cases shows only 28% difference between the maximum and minimum pressure obtained at depth 1.44 m.

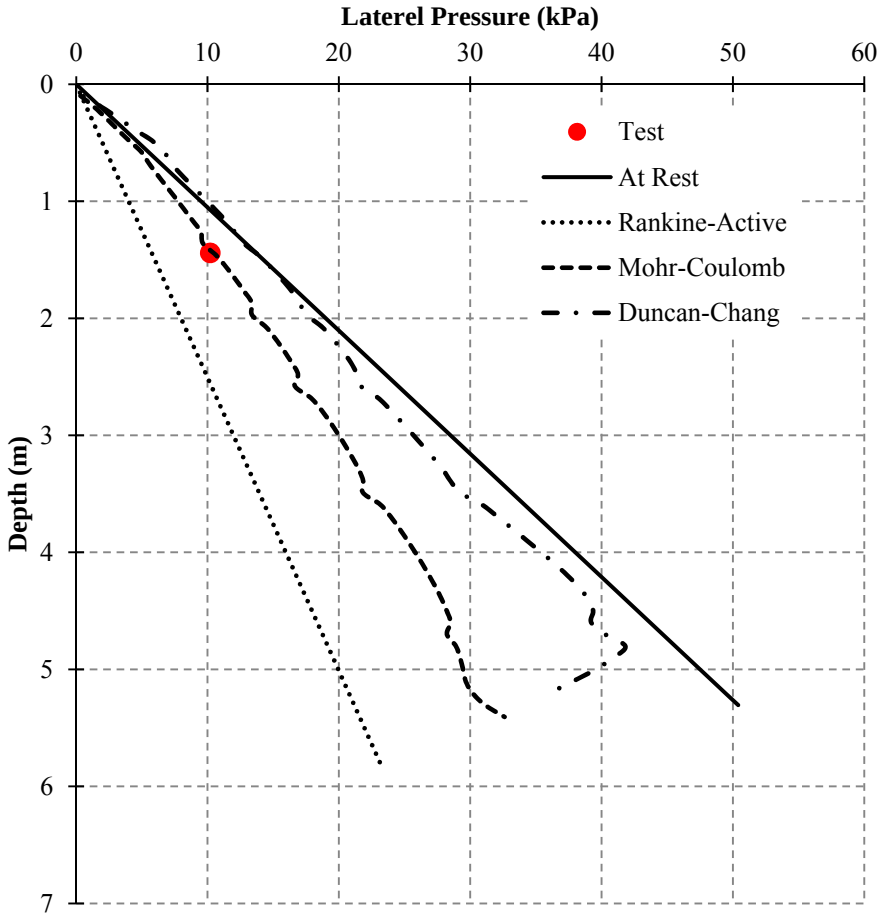

Figure 4-8: Lateral earth pressure in depth

4.3.4 Moment in Manhole Base

Manhole base is one of the critical parts of the manhole structure due to experiencing tension resulted from the induced moment. The critical moment that concrete experiences before the formation of cracks can be calculated by knowing the modulus of rupture in concrete. In order to avoid crack formation in the manhole base, the moment in the base due to existing loads must be calculated. This moment can be calculated by using the clamped plate theory (18). The clamped plate theory calculates

the radial and angular moment (M_r and M_θ) in a circular clamped plate with radius "R" under uniform pressure of "p" at a distance of "r" as:

$$M_r = \frac{pR^2}{16}\left[(1+\upsilon) - (3+\nu)\frac{r^2}{R^2}\right] \quad (4)$$

$$M_\theta = \frac{pR^2}{16}\left[(1+\upsilon) - (1+3\nu)\frac{r^2}{R^2}\right] \quad (5)$$

The above equations indicate that the maximum moment occurs at the center of the disk and it is equal to:

$$M_{max} = \frac{pR^2}{16}(1+\upsilon) \quad (6)$$

Figure 4-9 compares the bending moment in the manhole base calculated by the clamped plate theory with the results obtained from ABAQUS using DC and MC material models for soil. The pressure used for calculating the moment is the average pressure beneath the manhole base obtained from simulation. In both cases of simulation, the maximum bending moment which is located at the center of the manhole base is in good agreement with the calculations from the clamped plate theory. By getting closer to the edges, the results from the simulation differ from the results from calculations which can be due to the fact that the manhole base is not acting like a clamped plate and some movements may occur at the edges. Comparison of the maximum moment obtained from PLAXIS simulation (7) performed and reported by Sabouni et al. is also shown in Figure 4-9. There is a 32% difference between the results which can be due to a difference in magnitude of the pressure under the manhole base from different simulations. Moments in cases of using two different material models for soil are almost the same.

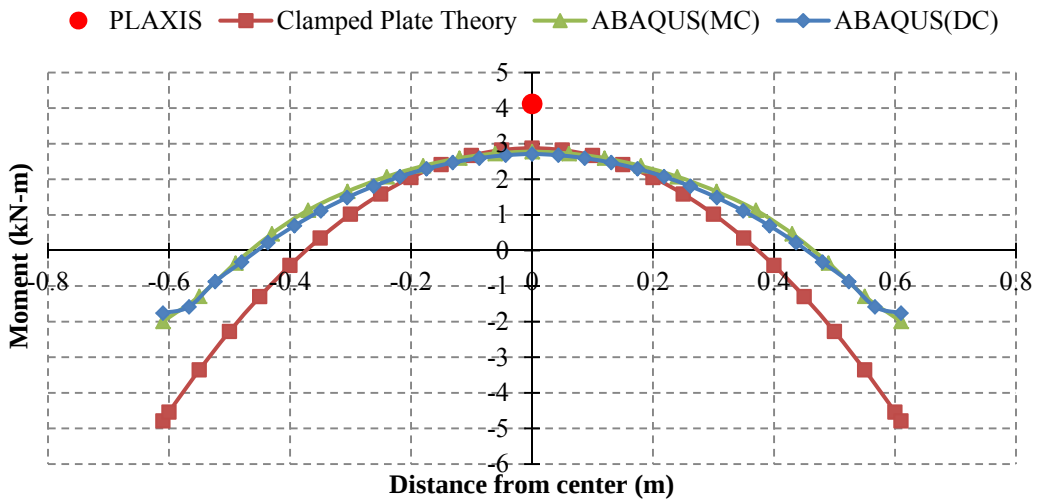

Figure 4-9: Moment in manhole base

Cracking moment in the manhole base can be calculated by using Eq. (7) (19), in which f_r is modulus of rupture for concrete, I_g is moment of inertia of the section and y_t is distance from centroid axis of gross section.

$$M_{cr} = \frac{f_r I_g}{y_t} \tag{7}$$

The calculations show that the cracking moment is about 10.8 kN-m/m, which is greater than the existing moment in manhole base.

4.3.5 .Pipe Under Uniform Peripheral Pressure

4.3.5.1 Elastic Theory Solution for Pipe Under Pressure

To validate the finite element simulation of pipe under pressure discussed previously, theory of elasticity is used. According to this theory, radial and angular stresses at any distance of "r" from center in a hollow cylinder with inside diameter of "a" and outside diameter of "b" under peripheral pressure of "P" can be obtained using Lame's formulas (17):

$$\sigma_{rr} = -P\frac{1-\left(\frac{a}{r}\right)^2}{1-\left(\frac{a}{b}\right)^2},\ \sigma_{\theta\theta} = -P\frac{1+\left(\frac{a}{r}\right)^2}{1-\left(\frac{a}{b}\right)^2} \tag{8}$$

And radial deformation is calculated by:

$$u_r = \frac{1-\nu}{E}\frac{-b^2P}{b^2-a^2}r - \frac{1+\nu}{E}\frac{a^2b^2P}{b^2-a^2}\frac{1}{r} \quad (9)$$

Using the above theory and creating an elastic model of the pipe in ABAQUS, the analytical solutions are compared to the simulation results and the model is verified.

For the composite pipe by considering it as two pipes, one inside the other, and using the elasticity theory to calculate the deformation of two pipes at point C as shown in Figure 4-10, the pressure transferred to the inside pipe can be calculated. The procedure is to calculate the radial deformation of both pipes at point C and make them equal and solve the equation for outside pressure applied to the inner layer. Results are shown in Figure 4-10.

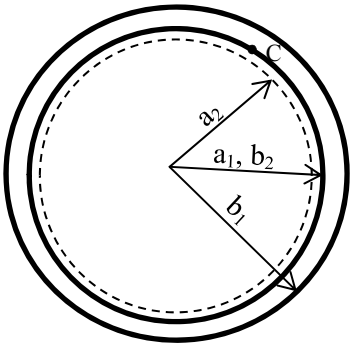

$$P' = \frac{-2E_2P}{E_1}\frac{b_1^2(b_2^2-a_2^2)}{(\nu_2(b_2^2-a_2^2)-b_2^2-a_2^2)(b_1^2-a_1^2)}$$

P = Pressure on outside pipe
E_1, E_2 = Modulus of elasticity of outside and inside pipe
v_2 = Poisson's ratio of inside pipe

Figure 4-10: Composite pipe under pressure

Comparing the results from simulation of the composite pipe with elastic materials to the analytical solution can verify the simulation. The results from simulation and analytical solution for bare and lined concrete pipes with elastic material properties at selected points are presented in Table 4-3. The results are in good agreement as shown in the table.

Table 4-3 Comparison of the analytical and simulation results for elastic pipe under peripheral pressure

		r(cm)	u_{rr}(mm)	σ_{rr}(MPa)	$\sigma_{\theta\theta}$(MPa)	%Diff
Concrete Pipe	Analytical	30.48	0.787	0	-76.61	0.013
	ABAQUS		0.787	-0.0006	-76.6	
	Analytical	34.54	0.762	-8.48	-68.12	0
	ABAQUS		0.762	-8.5	-68.12	
Composite Pipe	Analytical	29.84	0.787	0	-14.16	1.87
	ABAQUS		0.787	-0.0002	-14.43	
	Analytical	30.48	0.787	-0.29	-13.87	1.84
	ABAQUS		0.787	-0.29	-14.13	

4.6 Finite Element Modeling of Epoxy-Lined Manhole

Regarding the above discussion, the generated models in ABAQUS are verified and can be used for further study on rehabilitated manhole structure with epoxy lining. In order to simulate the deteriorated manhole structure, it is assumed that deterioration of concrete results in reduction of the structure's stiffness. There are several articles in the literature, which discuss the mechanical properties of deteriorated concrete and in all of them without considering the reason for deterioration, Young's modulus of the concrete decreases(20)–(21). As a result, in this study, stiffness reduction was simulated by decreasing the Young's modulus of the concrete. Three different manhole conditions are considered in this research. The first case is the manhole without any deterioration as a base for comparison; the second case is a partially deteriorated manhole structure which is simulated by decreasing Young's modulus of concrete to one tenth of its original value and in the third case, which is the worst case scenario, the manhole structure concrete is replaced by the surrounding soil. In the latter case it is assumed that the concrete is fully deteriorated and loads are carried by epoxy lining. In both deteriorated cases, a layer of 6

mm epoxy liner was applied to the inside of the manhole. The interaction between the coating and concrete was considered frictional behavior with a friction coefficient of 0.5 in tangential behavior and hard contact in normal behavior.

For all three cases, three different load configurations are applied to the manhole structure. The first load configuration only considers soil pressure around the structure. In this condition, it is assumed that the water table is located under the manhole base and there is no traffic load on the ground surface. In the second load configuration, the water table rises to ground surface and water pressure is applied to the manhole structure as well as the soil pressure. In the third load configuration, traffic load is applied on the ground surface in addition to soil and water pressure.

To apply the traffic load to the manhole structure ASTM-C890 (22) is used. In this standard the vehicle and pedestrian load designation are as presented in Table 4-4.

Table 4-4 Vehicle and Pedestrian Load Designations

Designation	Load, max	Uses
A-16	71.17 kN per wheel	Heavy traffic
A-12	53.38 kN per wheel	Medium traffic
A-8	35.58 kN per wheel	Light traffic
A-03	14.36 kPa	Walkways

In this standard it is also mentioned that distribution of wheel loads through earth fills are considered below ground structure where backfill separates the vehicle wheels and the top surface of the structure will be like a truncated pyramid as shown in Figure 4-11 and the loaded area will be:

$$A = (W + 1.75H) \times (L + 1.75H) \quad (10)$$

where:

A= wheel load area, m^2,

W= wheel width, m,

L= wheel length, m,

H= height of backfill between wheels and structure, m

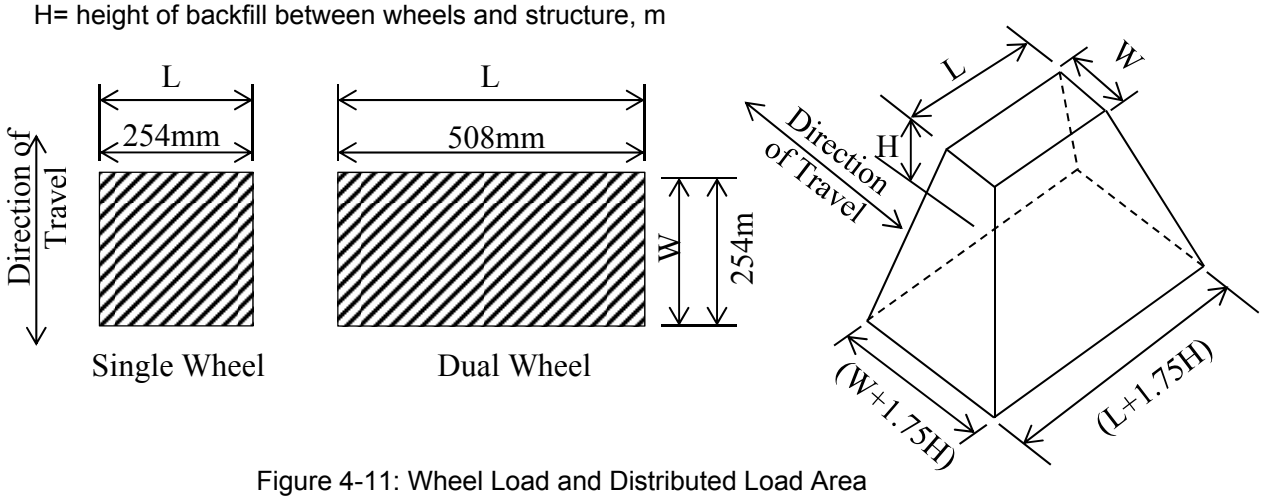

Figure 4-11: Wheel Load and Distributed Load Area

In order to do the traffic load simulation a dual wheel load area with a backfill height of 15.2 cm is considered. Using the above equations and assuming a medium traffic with a maximum load of 53.38 kN per wheel the total pressure on the soil surface due to traffic will be:

$$P = \frac{53.38}{(0.254+1.75*0.15)(0.508+1.75*0.15)} = 134.16\ kPa \quad (11)$$

As a result, a distributed load of 135 kPa is applied in a width of 0.77 m representing dual wheel load traffic on the surface right on the manhole cover. Since the cover is not simulated in the current model the load carried by the cover is calculated and applied on the manhole wall.

4.7 Results and Discussion

The results of manhole simulation under different load configurations for three cases, one sound concrete and two deteriorated concrete, are presented as follows. In this part, Case I refers to the manhole structure with sound concrete, Case II represents a partially deteriorated manhole structure with a Young's modulus value that is one tenth that of the original Young's modulus of concrete and Case III refers to manhole structure with fully deteriorated concrete.

Comparison of the results for Case II with and without epoxy liner inside the deteriorated manhole structure does not show significant difference, which means that according to the existing loads and manhole condition, the 6 mm epoxy lining does not affect structural behavior of the partially deteriorated manhole.

In Case III, the manhole structure can only carry the load from soil pressure. The results from this simulation with and without epoxy lining are presented separately.

4.7.1 Manhole Under Soil Pressure

Pressure distribution on manhole structure and its deformation due to surrounding soil pressure are shown in Figure 4-12. Both soil material behavior, Duncan-Chang (DC) and Mohr-Coulomb (MC) are considered in this simulation. Comparison of the results shows that decreasing the stiffness of the manhole reduces the pressure acting on the manhole structure, which is due to an increase in deformation of the manhole wall.

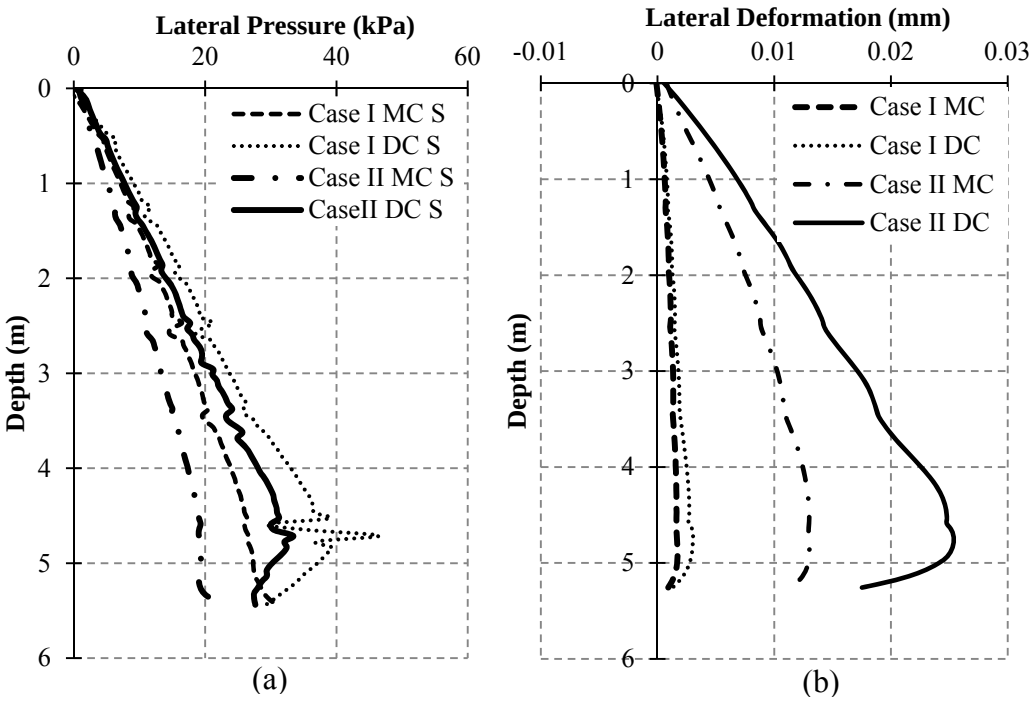

Figure 4-12: Manhole under soil pressure: (a) pressure on manhole structure and (b) horizontal deformation of manhole structure

4.7.2 Manhole Under Soil and Water Pressure

For this load configuration the water table is assumed to be on the ground surface, and the manhole structure carries the pressure from soil and water at the same time. Pressure distribution and deformation of the manhole are shown in Figure 4-13. As expected by adding the water pressure on manhole structure in all cases, the lateral pressure and deformation of the manhole wall increased.

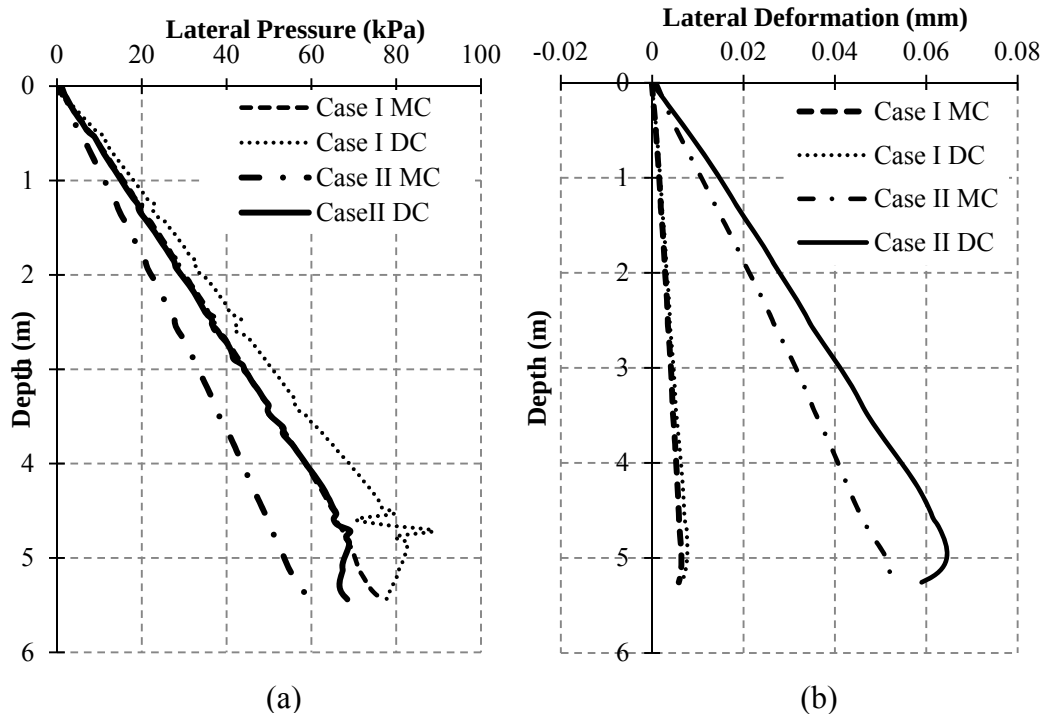

Figure 4-13: Manhole under soil and water pressure: (a) pressure on manhole structure and (b) horizontal deformation of manhole structure

4.7.3 Manhole Under Soil and Water Pressure and Traffic Load

The last load configuration considers soil, water and traffic load on top of the manhole structure at the same time. This loading case is the most critical case. Pressure and deformation in depth are shown in Figure 4-14. In this case due to the traffic load on the manhole, the lateral pressure at depth zero is not zero, and there is a lateral deformation on manhole wall on the ground surface.

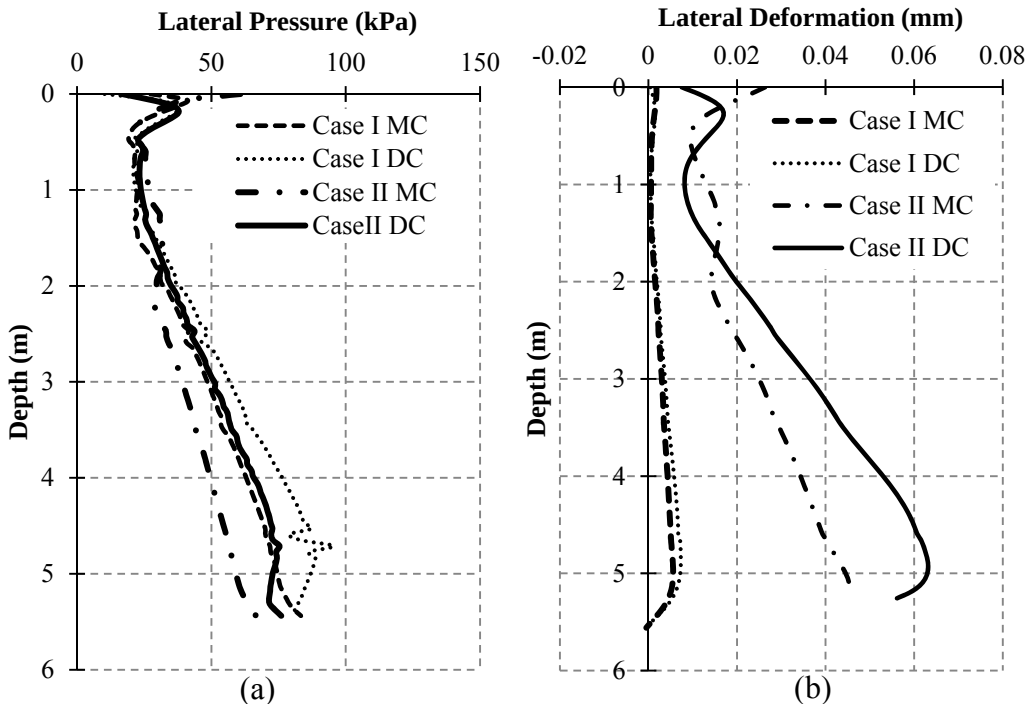

Figure 4-14: Manhole under soil and water pressure and traffic load: (a) pressure on manhole structure and (b) horizontal deformation of manhole structure

To compare the results from different load configuration for Case I and Case II, lateral pressure distribution and lateral deformation of the wall for these two cases are shown in Figure 4-15 and Figure 4-16 separately. For traffic load configuration lateral pressure and deformation starts at the ground surface. In Figure 4-15 and Figure 4-16, “S” represents soil pressure load, “SW” represents soil and water pressure load and “SWT” is representative of soil and water pressure along with traffic load combination.

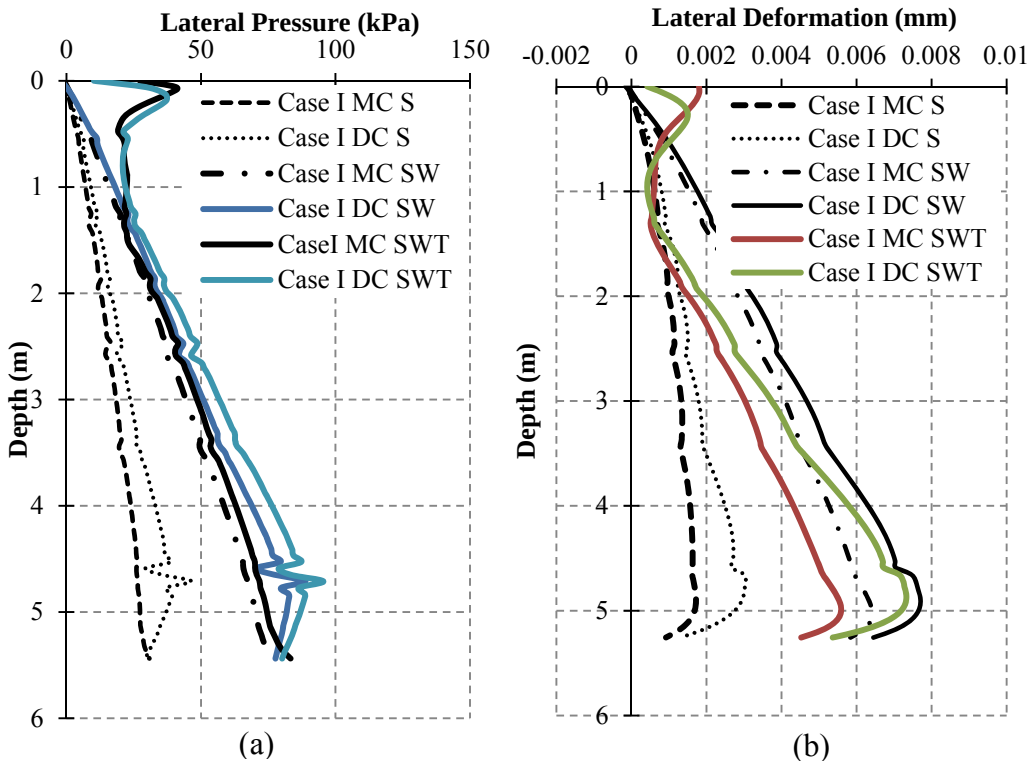

Figure 4-15: Sound manhole under different load configurations: (a) pressure on manhole structure and (b) horizontal deformation of manhole structure

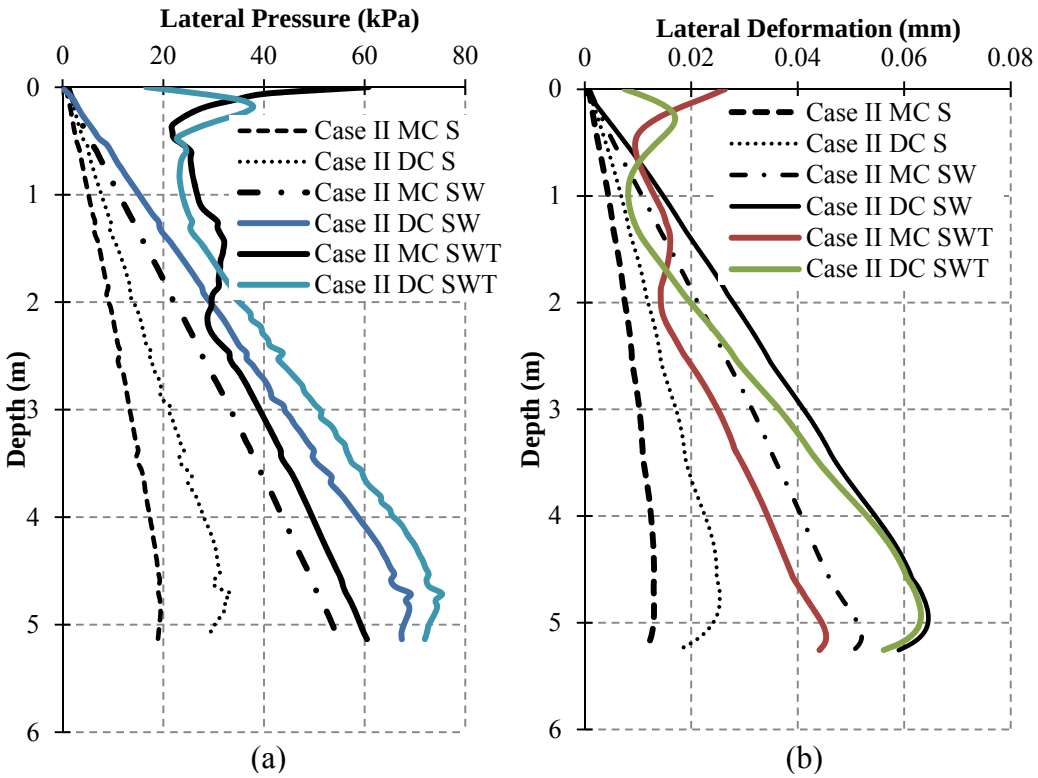

Figure 4-16: Deteriorated manhole under different load configurations (a) pressure on manhole structure and (b) horizontal deformation of manhole structure

4.7.4 Case III

As mentioned before, in this case the manhole structure is assumed to be fully deteriorated and the epoxy lining carries the entire load. After replacing the material properties of the concrete with material properties of the soil, the manhole structure fails due to soil pressure. Adding the epoxy lining inside of the deteriorated manhole structure slightly changes the deformation of the structure as shown in

Figure 4-18. Formation of the plastic zones in the soil and manhole structure due to surrounding soil pressure is shown in Figure 4-17. For this case, due to soil failure, water pressure and traffic load cannot be applied.

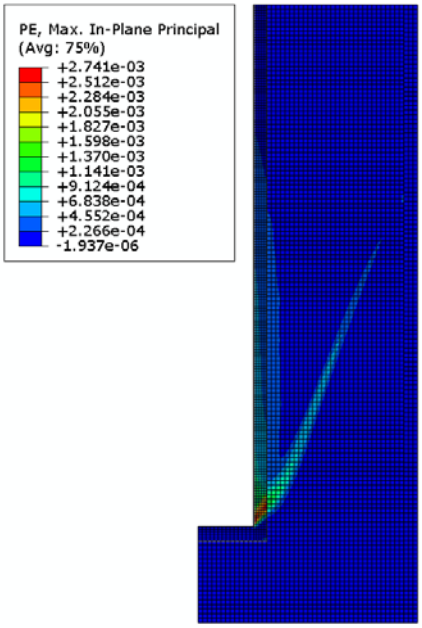

Figure 4-17: Soil failure in Case III

Comparison of the results obtained from this case before and after applying the epoxy lining inside of the manhole structure is presented in

Figure 4-18. As shown, compared to the other two cases, the pressure acting on the manhole structure has decreased significantly and deformation has increased. Applying the epoxy lining inside of the fully deteriorated manhole structure decreases the manhole deformation. For instance, at a 3 m depth, a 30% reduction in radial deformation is measured in the manhole structure.

In order to see the effect of increasing the thickness of the epoxy liner, a simulation is performed for Case III with a 12 mm epoxy liner. As expected, increasing the thickness results in a reduction in radial deformation of the deteriorated manhole structure by 36% compared to the 6 mm epoxy liner.

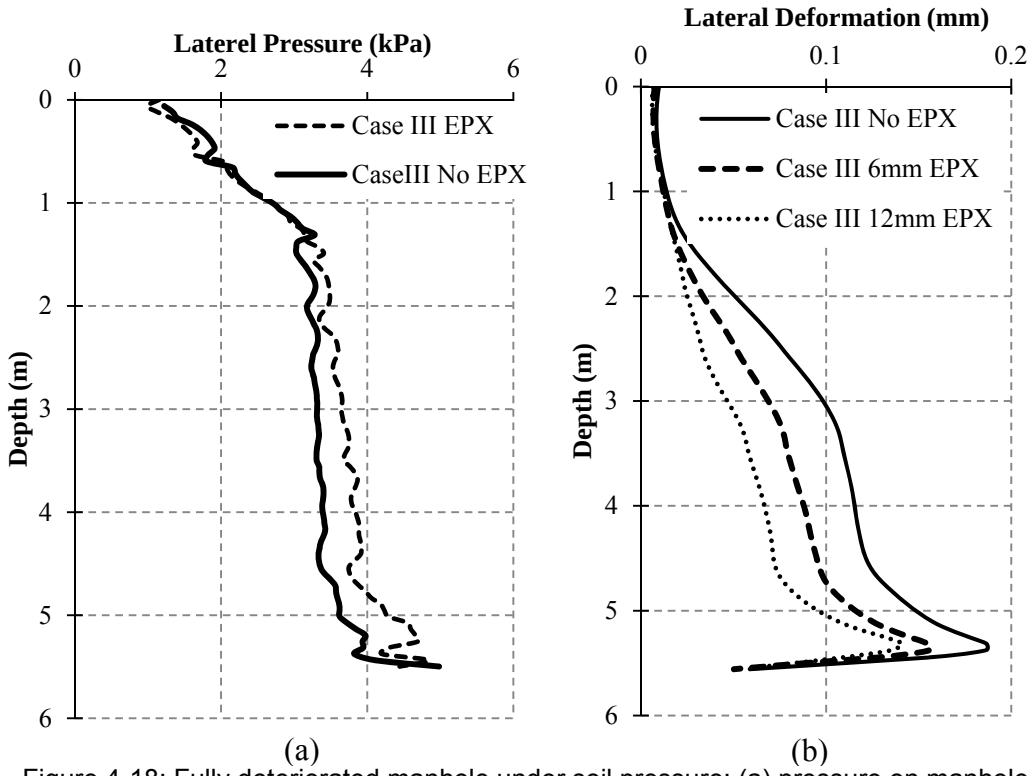

Figure 4-18: Fully deteriorated manhole under soil pressure: (a) pressure on manhole structure and (b) horizontal deformation of manhole structure

4.7.5 Manhole Base

For all of the cases above the moment in the manhole base decreases compared to the results presented in Figure 4-9 which shows the moment for manhole without any deterioration. As a result, the existing moment in the manhole base for current study is not critical.

4.8 Conclusions

A calibrated model of a precast concrete manhole structure was generated in ABAQUS finite element software. This model was used to study the effect of applying a 6 mm layer of epoxy lining inside of a manhole structure with different degrees of deterioration. Behavior of the structure under different loading configurations was studied. The results show that for a partially deteriorated manhole structure, the presence of an

epoxy lining does not have any significant effect on radial deformation and lateral pressure acting on the manhole structure. In the case of a fully deteriorated manhole, the structure carries only the soil pressure and fails without adding water pressure or traffic load. In this case the epoxy lining decreases radial deformation by 30%, and can slightly postpone failure of the manhole structure. According to the current study, a 6 mm epoxy lining does not have any significant effect on behavior of a manhole under presented loading configurations and specified dimensions. Increasing the thickness of the liner by two times resulted in a smaller radial deformation in the case of a fully deteriorated manhole.

References

1. Najafi M, Gokhale S. Trenchless technology : pipeline and utility design, construction and renewal. New York: McGraw-Hill; 2005.

2. Dr. Ray Sterling LW, Robert Morrison,. Rehabilitation of WastewaterCollection and WaterDistribution Systems WHITE PAPER. USEPA; 2009 EPA/600/R-09/048.

3. Dan Ellison FS, Peter Oram, Will Lovins, and Andrew Romer,Steven J. Duranceau,Graham Bell. Global Review of Spray-On Structural Lining Technologies. 2010.

4. Redner JA, Hsi, R.P., Esfandi, E.J., Sydney, R., Jones, R.M., Won, D., and Andraska, J. Evaluation of Protective Coatings for Concrete. County Sanitation Districts of Los Angeles County W, CA; 2004.

5. IKT. Rehabilitation of waste water manholes: Large scale tests and in-situ studies. 2012.

6. Sabouni R, El Naggar MH. Circular precast concrete manholes: experimental investigation. Canadian Journal of Civil Engineering. 2011;38(3):319-30.

7. Sabouni R, El Naggar MH. Circular precast concrete manholes: numerical modeling. Canadian Journal of Civil Engineering. 2011;38(8):909-20.

8. Matthews J, Condit, W., Wensink, R., Lewis, G. Performance evaluation of innovative water main rehabilitation cured-in-place pipe lining product in Cleveland, OH. AGENCY USEP; 2012 241308 Contract No.: EPA/600/R-12/012.

9. Mohammad Najafi VFS. STRUCTURAL CAPABILITIES OF NO-DIG MANHOLE REHABILITATION. 2015.

10. Sabouni R. Experimental Investigation & Numerical Modeling of Concrete Manholes. School of Graduate and Postdoctoral Studies: The University of Western Ontario; 2008.

11. Association MoToOaME. Construction specification for excavating, Backfilling, and compacting for maintenance holes, catch basins, ditch inlets, and valve chambers Ontario Provincial Standard Specification. Ontario, Canada2013.

12. Duncan JM, Chang C-Y. Nonlinear analysis of stress and strain in soils. Journal of the soil mechanics and foundations division. 1970;96(5):1629-53.

13. Kondner RL, Zelasko JS. Void ratio effects on the hyperbolic stress-strain response of a sand. Laboratory shear testing of soils: ASTM International; 1964.

14. Janbu N. Soil Compressibility as Determined by Oedometer and Triaxial Tests. European Conference on Soil Mechanics & Foundations Engineering; Wiesbaden, Germany1963. p. 19-25.

15. Dong W, Hu L, Yu YZ, Lv H. Comparison between Duncan and Chang's EB Model and the Generalized Plasticity Model in the Analysis of a High Earth-Rockfill Dam. Journal of Applied Mathematics. 2013;2013:12.

16. Hibbit, Karlsson, Sorensen. ABAQUS/Standard Analysis User's Manual: Hibbit, Karlsson, Sorensen Inc.; 2007.

17. Saada AS. Elasticity: theory and applications: Elsevier; 2013.

18. Reddy JN. Theory and analysis of elastic plates and shells: CRC press; 2006.

19. ACI. Building Code Requirements for Structural Concrete(ACI318-95). Farmington Hills, MI1995.

20. Zhang B, Wu K. Residual fatigue strength and stiffness of ordinary concrete under bending. Cement and concrete research. 1997;27(1):115-26.

21. Xiao J, Xie M, Zhang C. Residual compressive behaviour of pre-heated high-performance concrete with blast–furnace–slag. Fire Safety Journal. 2006;41(2):91-8.

22. Standard Practice for Minimum Structural Design Loading for Monolithic or Sectional Precast Concrete Water and Wastewater Structures. ASTM International; 2013.

Chapter 5

5.1 Conclusion

In this research after analyzing the test results from coated and uncoated concrete beams and pipes, the effect of coating material on the structural behavior of different concrete members was studied. The results from the tests were used to develop calibrated finite element models of beams, pipes and manholes. The finite element models were used to predict behavior of each concrete member under different loading configurations with different lining thicknesses and material.

Flexural strength tests on coated and uncoated concrete beams showed an increase of 10% in the peak load after adding the lining material.

Three-edge bearing tests on lined and unlined concrete pipes showed a wide range of increase in the peak loads depending on the type and thickness of the lining materials. The finite element model was generated for some of the test results and a parametric analysis was performed on the generated model.

The selected results from three-edge bearing test showed that adding a 6 mm-thick liner to the concrete pipe increases the measured peak load by 30%.

The results of the parametric analysis for D-load configuration on the effect of lining thickness on peak load confirmed that for 3 mm, 6 mm, and 12 mm thicknesses, 7%, 37%, and 75% increases in the peak load occurred, respectively.

Radial deformation variation for different degrees of deterioration of concrete showed an 82% and 182% increase in radial deformation by decreasing Young's modulus of concrete to 50% and 30% of its original value when no lining was applied inside of the pipe. For a 12 mm lining, radial deformation increased by 57% and 116% for 50% and 30% of the original Young's modulus, respectively.

By decreasing the Young's modulus of the lining to 50% of its original value, a 14% reduction in peak load for 3 mm and 12 mm lining thicknesses was measured while the radial deformation at the peak load did not change.

The effect of applying epoxy lining inside of the manhole structure with different degrees of deterioration under soil, water and traffic load shows that for a partially deteriorated manhole, the epoxy lining did not significantly affect radial deformation of the deteriorated structure. Comparison of the results for a partially deteriorated manhole structure with epoxy lining under different loading configurations shows that adding the water and traffic load increased lateral deformation and lateral pressure acting on the manhole structure by three times. In the case of a fully deteriorated manhole structure, the composite structure was only capable of carrying soil pressure, and it failed before adding water pressure to the structure. For this case, the epoxy lining decreased radial deformation by about 20%. Increasing the thickness of the lining from 6 mm to 12 mm, resulted in a 22% smaller deformation in the case of a fully deteriorated manhole structure.

5.2 Recommendations for Future Study

For further consideration of the effect of polymeric lining on the structural behavior of different concrete members, the following recommendations are proposed:

- Flexural tests can be performed on deteriorated concrete beams to study the effect of coating materials on improvement of flexural behavior of deteriorated concrete samples.
- Buried concrete pipes with and without linings can be instrumented to study the behavior of resultant composite pipe under actual field conditions.
- The developed model for pipe can be used to create a design criterion for polymeric coated concrete pipes.

- Due to the lack of study on full scale deteriorated manhole structures, research can be performed by instrumenting an existing deteriorated manhole structure before and after applying epoxy lining under existing loads to study the behavior of the composite structure in the field.
- The generated manhole model can be used to study the behavior of composite manhole structures with different depths to obtain the effect of manhole depth on the performance of the rehabilitated structure.

Biographical Information

Elmira Riahi received her bachelor's degree in civil engineering from Sharif University of Technology, Tehran, Iran, in 2005 and her master's degree in geotechnical engineering in 2008 from the same university. Her MS research program focused on finite element modeling of tunnel construction stages and effect of water pressure on structures. She has been working for three years in geotechnical and structural consulting firms in Tehran, Iran. In fall 2012 she started her PhD program under supervision of Dr. Xinbao Yu at the University of Texas at Arlington (UTA) in the United States. During her study she worked as a research assistant, teaching assistant, and instructor for UTA undergraduate students. Her research focused on trenchless rehabilitation of underground infrastructures by using experimental and finite element modeling. Her research interest is soil-structure interaction and finite element modeling. She successfully completed all the course work and research for the degree of Doctor of Philosophy in Civil Engineering in July, 2016.